Journal of Materials Chemistry C

ROYAL SOCIETY OF CHEMISTRY

REVIEW

View Article Online
View Journal | View Issue

Cite this: J. Mater. Chem. C, 2024, 12, 8188

Conjugated polymers with near-infrared (NIR) optical absorption: structural design considerations and applications in organic electronics

Tanzida Zubair,† Md Mahmudul Hasan,† Raul S. Ramos† and Robert M. Pankow *

Conjugated polymers (CPs) have revolutionized soft-matter electronics by enabling the manufacture of non-toxic, low-cost, and mechanically robust materials and devices for various technologies, including organic photovoltaics (OPV), electrochromic devices (ECDs), organic field effect transistors (OFET), and organic bioelectronics. Coupled with breakthroughs in synthetic chemistry and structure-function properties, the advancements in organic electronics have been firmly intertwined with CP structural developments. Recent research efforts have focused on the molecular engineering of CPs to broaden the optical absorption to the near-infrared (NIR) region (>750 nm) to enable new capabilities in photon harvesting for photovoltaics, optical switching and detection, thermal energy management, active camouflage, and to tune energy levels to achieve n-type and ambipolar charge transport. This review presents a comprehensive overview of the design and synthesis of CPs with NIR optical absorption, and it describes their incorporation in established and emerging device applications. A central focus throughout is how the polymer structures can be tailored specifically for each application with included strengths and shortcomings. An emphasis is placed on recent and emerging polymer structures with an outlook on areas for future work.

Received 4th April 2024,
Accepted 14th May 2024

DOI: 10.1039/d4tc01391c

rsc.li/materials-c

Department of Chemistry and Biochemistry, University of Texas at El Paso, El Paso, Texas 79968, USA. E-mail: rmpankow@utep.edu

† These authors contributed equally.

Robert M. Pankow

Robert M. Pankow received his BA in Chemistry from the University of California, Santa Barbara (2012) and his MS in Chemistry from California State University, Northridge (2015). He then earned his PhD in Chemistry under the guidance of Prof. Barry C. Thompson at the University of Southern California (2020). Robert then moved Northwestern University where he was an Intelligence Community Postdoctoral Fellow in the lab of Prof. Tobin J. Marks. Robert then began his independent career as an Assistant Professor in the Department of Chemistry and Biochemistry at The University of Texas at El Paso in August 2023.

1. Introduction

The prodigious advancements in conjugated polymer (CP) structural engineering over the last few decades have been directly coupled with the development of new synthetic methodologies for monomer functionalization, polymerization, and an improved understanding of the structure–function relationships that enable state-of-the-art performance metrics in electrochromic devices (ECDs),[1–4] organic photovoltaics (OPV),[5–8] organic photodiodes and phototransistors (OPD and OPTs),[9–12] organic field effect transistors (OFET),[13–16] and organic electrochemical transistors (OECTs).[17–20] Recently, significant research effort has been focused on the development of CPs with near-infrared (NIR) optical absorption (750–2500 nm) to increase light harvesting capabilities in OPV,[21,22] provide optical transparency for smart-windows and photovoltaic green houses,[23,24] enable new capabilities in active camouflage,[25,26] provide discrete, transparent electronics,[27,28] and narrow bandgaps to enable ambipolar charge transport.[14,29,30] Compared to their inorganic counterparts possessing NIR-IR optical absorption, *e.g.* bulk III–V semiconductors,[31,32] quantum dots,[33] and 2D materials,[34,35] NIR-CPs are overall more sustainable and relatively non-toxic, are mechanically robust (flexible and stretchable), and provide ease of tuning the optical, electronic, and physicochemical properties.[36]

In previous decades, significant research effort in NIR-CPs was focused on developing new light harvesting polymers for

applications in polymer-fullerene organic solar cells, where the development of a polymer spectral response complimentary to fullerene and covering the visible wavelength range (380–700 nm) was primarily targeted.[37,38] Additionally, for ECDs CPs with optical switching and coloration within the visible wavelength range were heavily pursued, since this boasted the greatest benefit for smart-window and display technologies.[1,39] A characteristic of narrow bandgap CPs is ambipolar and n-type charge transport, which has been of great interest in OFET and OECT technologies, and the advent of electronic skin (e-skin) has stimulated renewed interest for NIR-CPs.[40,41]

In this review, the relevant aspects of NIR-CP design and their impact on the optical, electronic, and morphological/microstructural properties are first introduced. This includes ECDs, OPVs, OPDs, OPTs, OFETs, and OECTs. Next, different classes of NIR-CPs organized by repeat unit are provided with their distinct structural, optical and electronic characteristics, and critical synthetic steps, and aspects of sustainability indicated. While λ_{max} is used as a point of comparison for detailing the relative region of the polymer optical absorption profile, it is important to note that many of the NIR-CPs have optical absorption extending further beyond this value, so CPs with an optical bandgap (E_g) less than 1.65 eV where λ_{onset} = 750 nm are considered. Notable organic electronic device applications and relevant performance metrics are also indicated. An emphasis is placed on various electron acceptor repeat units in alternating donor–acceptor copolymers, since many of the unique developments and advancements in CP structure can be ascribed to this unit. Lastly, an outlook and concluding remarks are provided.

2. General considerations for NIR-CP design

The structural diversity present in NIR-CPs is the result of extensive materials evaluation and the establishment of structure–function relationships provided from evaluating device performance trends. In this section, we present key structural engineering strategies for the design and synthesis of NIR-CPs and provide an overview of factors influencing CP self-assembly, morphology and microstructure, and the specificity of these for different organic electronic device applications.

2.1 Donor–acceptor copolymers

The discovery of the donor–acceptor (D–A) copolymer by Havinga *et al.* ushered in a new era in CP structural design (see Fig. 1A).[42,43] Briefly, an alternating donor–acceptor conjugated copolymer consists of an electron donating unit and an electron accepting unit forming the π-conjugated backbone. The linkages and connectivity between these units are carefully controlled so that donor–donor (D–D) or acceptor–acceptor (A–A) homocouplings are minimized, which can be detrimental to achieving the desired optical and electronic properties.[44,45] This polymer design strategy can be further adjusted by incorporation of a second electron donor (yielding D1–A–D2–A) or electron acceptor unit (yielding D–A1–D–A2) to yield a semi-random terpolymer (Fig. 1A).[46] Following the principles of perturbation theory, by pairing an electron donor with a high lying highest occupied molecular orbital (HOMO) with an electron acceptor possessing a relatively low-lying lowest unoccupied molecular orbital (LUMO), the energy levels of the CP, *e.g.* the valence band and conduction band, can be dramatically altered to afford a narrow bandgap (Fig. 1A). Examples of donor (**1–7**) and acceptor (**8–12**) repeat units are provided in Fig. 1B, where it is shown that electron donating, *e.g.* electron rich aromatic heterocycles (**1–4**) or fused-ring aromatics (**5–7**), and electron accepting functionalities, *e.g.* electronegative heteroatoms and electron withdrawing substituents (**8–12**), are the defining structural features, respectively. Note, the utility of D–A copolymers was enabled by advancements in CP polymerization methods, such as the optimization of Suzuki–Miyaura and Stille polymerizations. These methodologies provide a high functional group tolerance thereby facilitating the rapid development of large libraries of polymer structures, due to the combinatorial screening and syntheses that can be easily accomplished when various donor comonomers are paired with various acceptors.[36,47,48] Thus, D–A copolymers with tailored bandgaps can be easily obtained providing either a wide optical bandgap ($E_g > 1.8$ eV), a medium bandgap (1.60 eV $< E_g <$ 1.75 eV), or a narrow bandgap ($E_g < 1.60$ eV).[7,49]

2.2 Heteroatom substitution, ring fusion, and π-extension

The strategic incorporation of halogens (*e.g.*, F or Cl), chalcogens (*e.g.*, Se or Te), or pnictogens (*e.g.*, N), is a simple yet powerful tool for narrowing the optical bandgap and tuning energetics to increase electron affinity and facilitate electron transport.[50–53] Examples of this are shown in Fig. 1C (**11–20**) starting from benzothiadiazole (BT). The incorporation of heteroatoms, such as fluorine and other halogens, can have profound effects on controlling the polymer morphology and self-assembly.[54] Notably, fluorination (**13**) and cyanation (**14**) have been shown to increase the electron affinity (EA), and halogenation can further improve the polymer conformational coplanarity *via* halogen-chalcogen and halogen-hydrogen non-covalent interactions.[55–58] The incorporation of other chalcogens in place of sulphur to afford other chalcogenophenes (**16**), such as selenophene and tellurophene, is an additional strategy for tuning the polymer optical/electronic and physicochemical properties.[53,59–61] Relative to thiophene, the inter-ring bond distances of selenophene and tellurophene are shorter indicating greater quinoidal character and improved π-orbital overlap within the π-conjugated system.[53,62,63] Thus, a reduction in the optical bandgap is observed. Additionally, strong Se–Se and Te–Te non-covalent interactions drive polymer self-assembly and can increase polymer semicrystallinity providing extended crystalline domains to accommodate charge transport.[63,64]

Next, ring fusion and π-extension (**17–20**) are additional strategies for rigidifying or increasing the extent of π-orbital overlap within the π-conjugated system of the CP, which in turn narrows the bandgap and facilitates charge transport.[65–67] In the case of ring-fusion for **11** this often invokes the functionalization of naphthalene and anthracene analogues and derivatives.

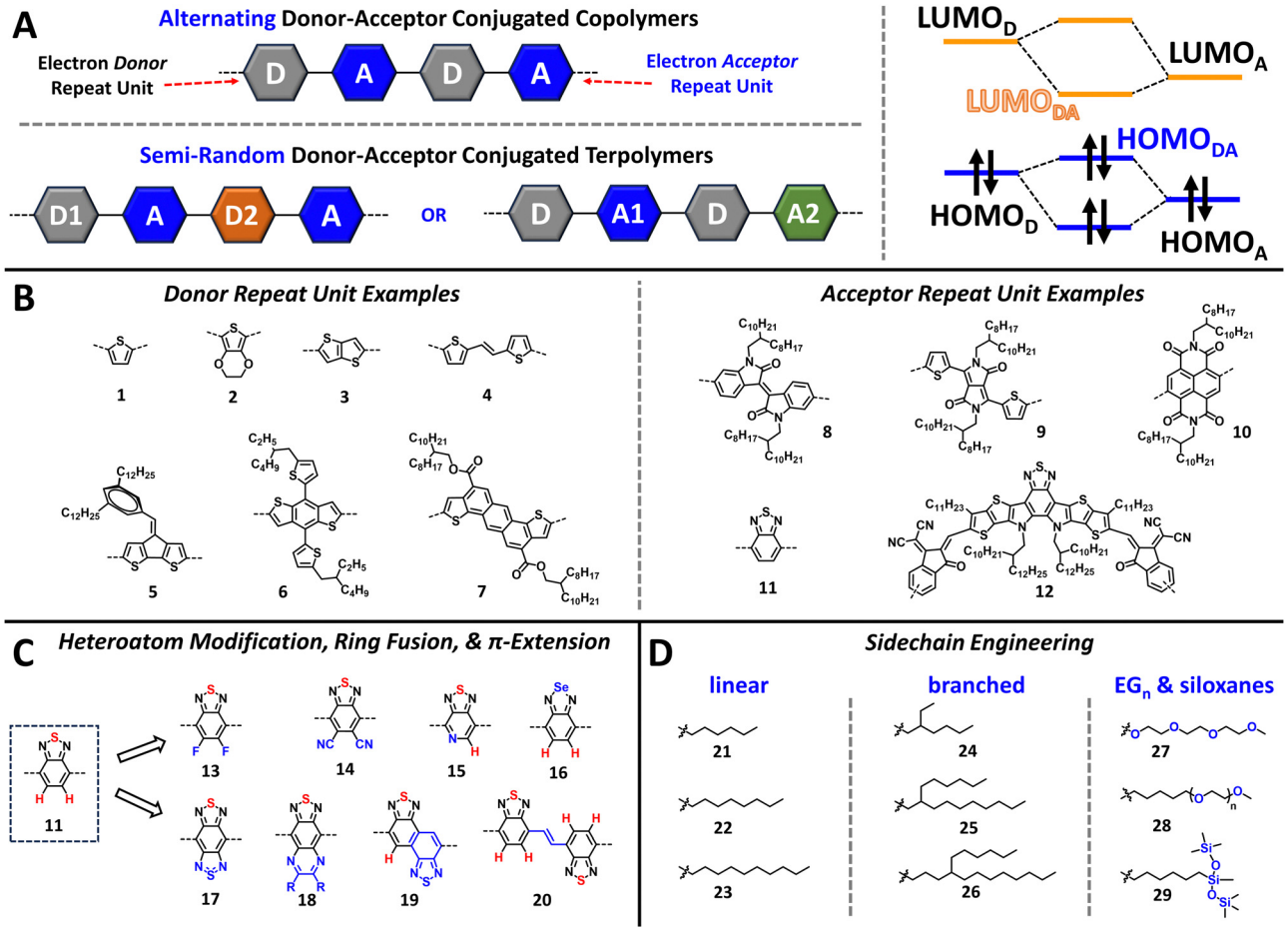

Fig. 1 (A) Overview of the donor–acceptor (D–A) conjugated copolymer and terpolymer design strategy towards the preparation of narrow bandgap conjugated polymers, and the mixing between donor monomer/acceptor monomer HOMOs ($HOMO_D$/$HOMO_A$) and LUMOs ($LUMO_D$/$LUMO_A$) to achieve a reduced bandgap (E_g = LUMO−HOMO). (B) Select examples of donor repeat units and acceptor repeat units to highlight the structural diversity and distinguishing functional groups that define these classes of monomers. (C) Examples of heteroatom modification, ring-fusion, and π-extension using benzothiadiazole (BT) as the example. (D) Examples of sidechain engineering including the design of linear alkyl, branched alkyl, and the incorporation of heteroatoms to afford oligo(ethylene glycol) (EG_n) and siloxane based sidechains.

However, extended fused ring monomers can also be synthesized from simpler molecular building blocks (**6**, **7**, and **12**) *via* linear or convergent synthetic pathways.[68–71]

2.3 Sidechain engineering

The CP sidechains facilitate solution processing and dictate the identity of processing solvent, *e.g.*, halogenated solvents (chloroform, chlorobenzene, or dichlorobenzene) or non-halogenated solvents (*e.g.*, toluene, xylenes, alcohols, ethers, and water).[72] In addition, they also direct the polymer self-assembly with direct influence over the polymer crystallization, aggregation, polymer chain entanglement, sidechain interdigitation, and polymer orientation relative to the substrate.[73–77] Thus, proper tailoring of the CP sidechains is imperative for achieving desired optical/electronic properties and device performance metrics.[72,78–81] Briefly, CP sidechains are often linear (**21–23**) or branched alkyl substituents (**24–26**) where linear sidechains provide increased sidechain interdigitation thereby affording CP crystalline domains with a high-degree of structural order (Fig. 1D).[82] Relative to their linear counterparts, branched alkyl sidechains provide improved polymer solubility in organic processing solvents, regulate polymer aggregation, and increase polymer chain entanglement.[83–85]

Lastly, the incorporation of heteroatoms within sidechains, such as oxygen and silicon, to yield oligo(ethylene glycol) (EG_n) or siloxane terminated sidechains (**27–29**) can impart solution processing with more polar solvents, such as alcohols and water, or more sustainable non-halogenated solvents (Fig. 1D), respectively.[86–89] Additionally, the incorporation of EG_n sidechains can provide improved electrolyte penetration and exchange, which is essential for ECDs and OECTs.[90–94]

2.4 Conjugated polymer morphology and microstructure

Precise control over the conjugated polymer morphology and microstructure is imperative for achieving desirable optoelectronic and charge transport properties and ultimately state-of-the-art performance metrics.[95–97] As mentioned before, CPs can self-assemble *via* non-covalent interactions directed by the heteroatoms present within the conjugated backbone and *via* sidechain interdigitation to form well organized lamellae.

Detailed in Fig. 2A, CP thin films can be comprised of a mixture of crystalline and amorphous domains where the crystalline domains are distinguished by improved polymer self-assembly and highly ordered nanostructuring. In contrast, the amorphous domains contain polymer chains with a random orientation and lack a well-defined microstructure. In a fully amorphous polymer, there is an absence of observable crystalline domains, and the polymer chains assume a random orientation (Fig. 2A). It is important to note that many semicrystalline CPs afford excellent charge transport properties, since the intermolecular and π–π interactions that facilitate charge delocalization and transport between polymer chains have an increased presence in the crystalline domain.[98] Note, amorphous polymers with well-defined electronic coupling between polymer chains are still capable of possessing efficient charge transport.[99]

Additionally, different organic electronic device applications require specific polymer morphologies and microstructures to achieve desirable performance. Specifically, for ECDs and OECTs, where device operation is tethered to the ability of the electrolyte to penetrate and exchange within the polymer film, having a CP with large crystalline domains can lead to electrolyte ion trapping which is detrimental to device performance.[92,100,101] Conversely, in OFETs having a large crystalline domain size can be beneficial to ensuring efficient charge transport and high hole and electron mobilities.[98,102,103] Larger crystalline domain sizes are also important in OPV, but in this setting the domain sizes must be carefully controlled to minimize extensive aggregation within the active layer blend to provide efficient photocurrent generation and charge extraction.[104,105] This concept of controlling the polymer blend morphology is detailed in Fig. 2A, where the different polymer constituents (polymer A and polymer B) can form separated domains and interpenetrating networks of crystalline and amorphous domains.[106,107] Lastly, the parameters influencing polymer self-assembly can dictate the orientation of the polymer chain, *e.g.*, whether the CP π-conjugated backbone is parallel or perpendicular to the face of the substrate (Fig. 2B). This orientational preference and the microstructural characterization described in Section 2.4 can be probed using grazing incidence wide-angle X-ray scattering (GIWAXS).[108,109] The polymer orientation is of critical importance to the device performance metrics for OFET and OPV, since the direction of polymer chain alignment indicates the preferred direction of charge transport. Specifically, a preferential π-face-on orientation facilitates charge transport in the vertical direction relative to the substrate face, which is beneficial for OPV. In contrast, an edge-on orientation facilitates charge transport in the horizontal direction, which is of greater utility to OFETs/OECTs. It is possible that preferential alignment is not observed in which case a bimodal or random orientation is obtained.[110]

To summarize, the D–A copolymer structure has enabled the rapid development of state-of-the-art NIR-CPs for a variety of organic electronic device technologies. Key functionalization strategies for tuning the polymer optical/electronic, physicochemical, and morphology and microstructure include heteroatom incorporation, ring fusion, π-extension, and sidechain engineering. Lastly, it is important to note that the different organic electronic devices each require a specific polymer morphology (semicrystalline or amorphous), microstructure, and chain orientation (π-face on, edge on, bimodal, or random), which is further elaborated upon in the following section.

3. Organic electronic device applications for NIR-CPs

In this section the basic overview of device operation and key performance metrics for ECDs, OPV, OPDs, OFETs, and OECTs

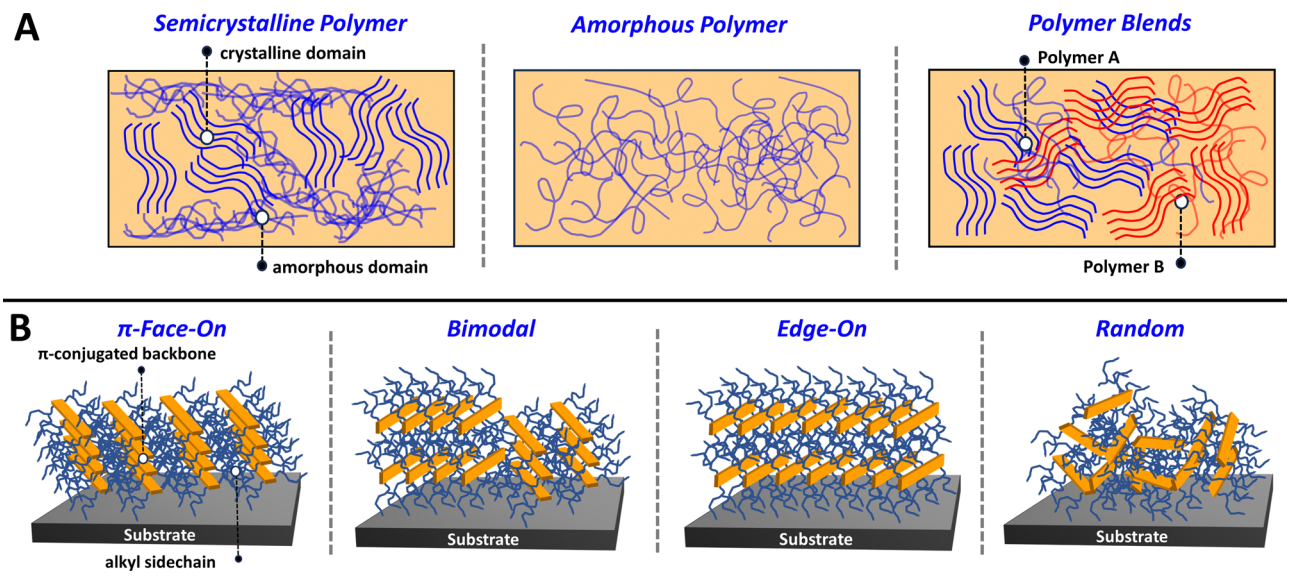

Fig. 2 (A) Depiction of the different semicrystalline and amorphous morphologies possible with conjugated polymers, as well as a depiction of a polymer blend composed of two semicrystalline polymers (polymer A and polymer B). (B) Depiction of the different polymer orientations relative to the substrate face, including: π-face on, bimodal, edge on, and random.

are briefly described to establish the broad utility of NIR-CPs and highlight the structural characteristics specific to each technology. Since the focus of this review is not on device physics or optimization of the device architecture, relevant reviews and articles detailing these topics are provided.

3.1 Electrochromic devices (ECD)

ECD technologies have traversed into new applications, including thermal energy management, energy storage and active camouflage, which traverse beyond the smart-window and display technology applications originally envisioned.[3,111,112] Central to these new capabilities for ECDs, are the advent of electrochemically robust NIR-CPs and advancements in ECD device architecture and engineering (Fig. 3).[111–113] For the vertical ECD architecture, a CP film is coated onto an optically transparent electrode and coated with an electrolyte. A second electrode coated with an ion-storage layer (ISL) covers the polymer CP film. For the lateral ECD architecture, the NIR-CP and the ISL are adjacent (in the same lateral plane), and each is coated with the electrolyte. Briefly, starting with a neutral CP a positive or negative bias is applied to electrochemically oxidize or reduce the CP layer, which in turn generates a p/n-polaron, respectively.[2,92,114] This leads to bleaching of the ground state optical absorption band and emergence of a polaron/bipolaron absorption band. Note, since this is an electrolyte coupled process, efficient and reversible electrochemical oxidation or reduction and electrolyte exchange within the CP layer are of critical importance. For NIR-IR optical switching, it is also important to consider the optical transparency of the electrode and substrate.[115] Key performance metrics for ECDs include the optical contrast ($\Delta T\%$), the switching time (t_{95}), coloration efficiency (CE), cycling stability, and optical memory.[2,111,114]

Specific for considerations for conjugated polymer design include incorporation of functionalities and repeat units that impart electrochemical robustness, such as 3,4-ethylenedioxythophene (EDOT), and oligo(ethylene glycol) (EG_n) sidechains to facilitate electrolyte penetration and exchange.[114] NIR-CPs for ECDs have been synthesized primarily *via* Stille polymerization, but it is notable that Reynolds *et al.* have demonstrated that CPs for ECDs can be prepared using direct arylation polymerization (DArP), which is more sustainable since it proceeds *via* C–H functionalization and avoids the use of toxic trialkylstannane residues.[116–119] In this review, NIR-CPs employed for ECDs include isoindigo (Section 4.1) and diketopyrrolopyrrole analogues (Section 4.2).

3.2 Organic photovoltaics (OPV)

OPV seeks to provide a sustainable energy capture resource to combat fossil fuel dependence, and broadening CP optical absorption into the NIR wavelength region has been a long-standing goal to enable efficient solar energy harvesting.[8,37,120] OPV device architectures are shown in Fig. 4 where the NIR-CP resides in the active layer. The active layer is a blend of an electron donor polymer (Fig. 5) and an electron acceptor small-molecule or an electron acceptor polymer (Fig. 8–12). This blend forms a bulk-heterojunction, which is a phase-separated interpenetrating bicontinuous network composed of the donor and acceptor domains or phases (see Fig. 2A).[121] Note, the active layer can also be composed of a single-component where the donor and acceptor are covalently linked, *e.g.*, single-component solar cells and double cable polymers.[122] The active layer is then interfaced with a hole and an electron transport layer, which are in contact with the electrodes used for charge collection. The nomenclature used (conventional or inverted), simply refers to whether the bottom electrode is in contact with the hole transport layer (conventional) or the electron transport layer (inverted). Briefly, device operation initiates when the donor polymer absorbs sunlight generating an exciton that travels to the donor–acceptor interface forming the charge-transfer (CT) state. Charge separation can then occur forming a hole and an electron in the donor and acceptor phases, respectively. These charges can then travel through the donor/acceptor domains until collected by the electrodes yielding photocurrent. Key performance metrics used for evaluating OPV device performance include the short-circuit current (J_{sc}), the open-circuit voltage (V_{oc}), fill-factor (FF), and the power conversion efficiency (PCE), which have been described in detail in relevant reviews.[123–126]

The design of donor and acceptor polymers for OPV is highly complex and requires the consideration various facets including: (i) the ionization potential (IP) and electron affinity (EA) of the donor polymer and acceptor polymer or small-molecule for efficient charge transfer and limiting charge recombination, (ii) ensuring complimentary optical absorption of the donor and acceptor to maximize spectral coverage, (iii) balanced and maximized hole and electron mobilities of the donor and acceptor, respectively, for efficient charge transport and collection, and (iv) optimal morphology/microstructure of the donor and acceptor phases to limit charge recombination/traps and maximize hole and electron charge transport to their respective

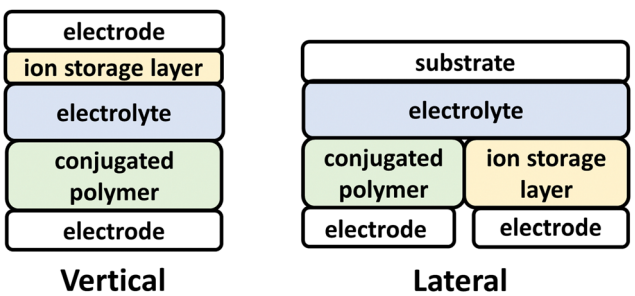

Fig. 3 Vertical (left) and lateral (right) ECD architectures.

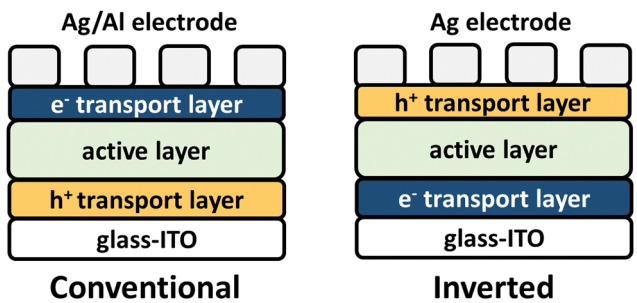

Fig. 4 Conventional (left) and inverted (right) OPV device architectures.

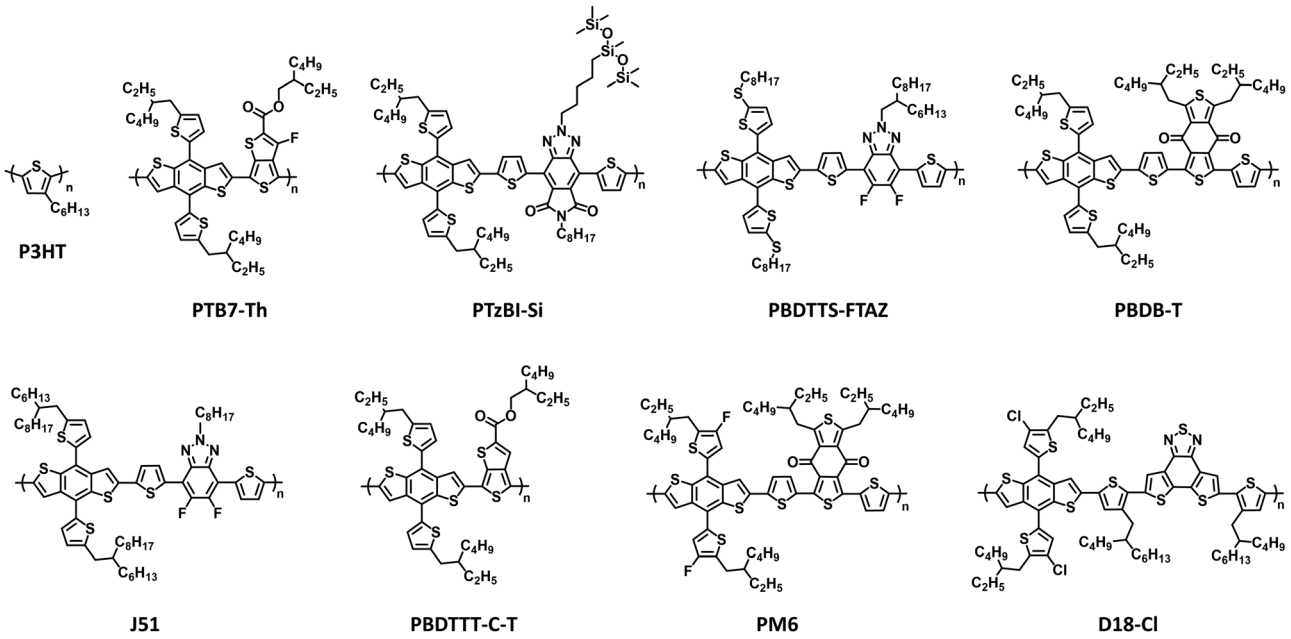

Fig. 5 Examples of donor polymers used in OPV, OPDs, and OPTs.

electrodes.[8,38,105] NIR-IR optical absorption has been targeted for both the donor and acceptor components, but recent state-of-the-art PCEs have been achieved by employing new polymer acceptors with NIR optical absorption and pairing with wide to mid-bandgap polymer donors.[5,6]

NIR-CPs for OPV are most often synthesized using Stille polymerization, since Stille affords broad functional group tolerance, high molecular weights (M_n), and polymer products with excellent structural fidelity. To avoid the generation of toxic tin waste and increase the sustainable aspects of OPV, there have been significant developments in the area of DArP and Zn-anion radical polymerizations to afford NIR-CPs that provide OPV performance metrics that converge or surpass their Stille analogues.[127–130] In this review, NIR-CPs incorporated into OPV devices include diketopyrrolopyrrole analogues (Section 4.2), naphthalene diimide (Section 4.3), benzothiadiazole (Section 4.4), polymerized small-molecule acceptors (Section 4.5), and cyclopentadithiophene analogues (Section 4.6).

3.3 Organic photodiodes (OPD)

OPDs seek to convert optical illumination into an electrical signal, and the incorporation of NIR-CPs has enabled new capabilities in optical sensing, biomedical imaging, and optical communication.[11,12] Note, organic photodetectors have various architectures, such as phototransistors (OPTs) and photoconductors, but only the photodiode architecture, which is analogous to the conventional and inverted OPV device architectures, is considered in this section (Fig. 4).[11] OPDs consist of an active layer analogous to OPV (blend of polymer donor and polymer or small-molecule acceptor), which has electron or hole transport layers above and below to ensure efficient charge transport and collection. The operation mechanism of an OPD is like that of OPV, where incident light is absorbed by the active layer leading to the formation of excitons, which in turn undergo charge separation and transport to the electrodes yielding photocurrent. Key figures of merit include the external quantum efficiency (EQE) at a given wavelength, the photocurrent/dark current ratio (P), the responsivity (R), and the detectivity (D), and the considerations for NIR-CP design are similar to that of OPV. Namely, the optical absorption of the active layer should overlap with the targeted wavelengths or ranges, and the energy levels of the donor polymer and acceptor polymer should be sufficiently offset to ensure efficient hole and electron charge separation. In this review, NIR-CPs incorporated into OPDs include benzothiadiazole (Section 4.4), polymerized small-molecule acceptors (Section 4.5), and cyclopentadithiophene analogues (Section 4.6).

3.4 Organic field effect transistors (OFET) and organic phototransistors (OPTs)

OFETs have enabled new capabilities in flexible and stretchable electronics, chemical/strain sensors, complimentary circuits, and electronic skin.[41,131–133] Briefly, the device architecture consists of a source and drain electrodes, the CP, which serves as the channel material, a dielectric layer, and a gate electrode (Fig. 6). These components can be arranged to afford a variety of different architectures, such as top gate bottom contact (TGBC), top gate top contact (TGTC), bottom gate bottom contact (BGBC), and bottom gate top contact (BGTC).[14,103] Device operation proceeds with application of positive or negative bias between the gate and source electrode (V_{GS}), which in turn polarizes the channel material and renders the OFET to its "ON" state. Application of a bias between the source and drain electrodes (V_{DS}) induces current flow through the channel and the drain current (I_D) is then measured.[103,134] Key performance metrics include the saturated current charge mobility (μ_{sat}), on/off current ratio (I_{on}/I_{off}), threshold voltage (V_{th}), and cycling stability. The operation of

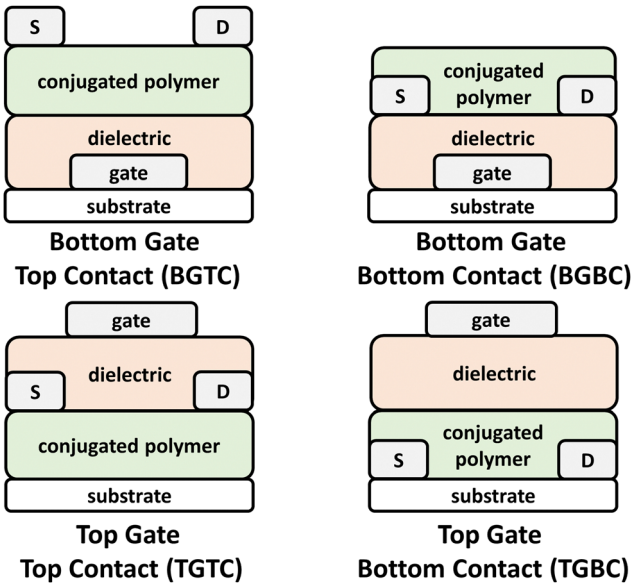

Fig. 6 Bottom gate top contact (BGTC), bottom gate bottom contact (BGBC), top gate top contact (TGTC), and top gate bottom contact (TGTC) OFET device architectures.

OPTs invokes a similar mechanism to OFETs, but optical absorption by the channel material (NIR-CP) modulates the charge carrier and transport properties leading to distinct metrics for channel current and threshold voltages between the illuminated and dark states.[135] As with OPDs, the key figures of merit for OPTs include P, R, and D.

Developments in transparent OFET technologies, NIR OPTs, and interest in high mobility n-type and ambipolar charge transport, which requires an increased EA, decreased IP, and therefore narrower bandgap, necessitates the pursuit of CPs with NIR optical absorption. However, unlike the previously described NIR-CP device applications, such as ECD, OPV, and OPD, the OFET operation mechanism does not directly depend on the optical absorption of the polymer. Additionally, the potential for these polymers to be employed in other organic electronic device applications outside of OFETs is significant, and so their inclusion within this review will hopefully catalyse these efforts.

As with OPV, there are numerous considerations regarding the overall structural design of CPs to achieve state-of-the-art performance metrics in OFET, *e.g.*, polymer morphology/microstructure and energy levels for charge transport. In general, highly crystalline polymers with short π–π distances, and a π-edge on orientation relative to the substrate are desired to achieve efficient charge transport. A notable structural optimization strategy for OFETs is sidechain engineering, where the inclusion of heteroatoms, such as silanes, and modification of the branching point in long chain branched alkyls provides efficient polymer packing and improved intermolecular π–π overlap.

NIR-CPs for OFETs are commonly synthesized *via* Stille polymerization, but more recently DArP as well as acid-catalysed aldol condensation-elimination and imine condensation polymerizations, which are tin and transition metal catalyst free, have afforded NIR-CPs with desirable performance metrics.[136,137] In this review, NIR-CPs incorporated into OFET and OPTs include diketopyrrolopyrrole (Section 4.2), naphthalene diimide (Section 4.3), and benzothiadiazole analogues (Section 4.4).

3.5 Organic electrochemical transistors (OECT)

Recently, OECTs have generated a resurgence of interest and have uncovered new frontiers in organic electronics and CP structural design. OECTs have numerous applications in biological sensors,[138] bioelectronics,[132,139] artificial synapses,[140] neuromorphic devices,[141,142] and complimentary circuits at the machine and biological tissue interface.[17,93,94] As with OFETs, the n-type and ambipolar charge transport imparted by narrow bandgap NIR-CPs have made these targeted polymers for OECTs. The OECT device architecture consists of source/drain electrodes, a gate electrode, and a conjugated polymer layer, but in place of the dielectric layer a liquid electrolyte (typically aqueous) is used (Fig. 7). Additionally, a polymer insulator, such as parylene, can be coated over the source/drain and the CP layer and the channel patterned using lithography. Common architectures include top contact, bottom contact, coplanar, and vertical. For OECTs operating in accumulation mode, application of a gate voltage (V_{GS}) is applied that induces the injection of the electrolyte ions and the electrochemical doping the channel material rendering the device to its "ON" state.[143] Key performance metrics for OECTs include the transconductance (g_m), voltage hysteresis (ΔV), on/off current ratio (I_{on}/I_{off}), and cycling stability.

For efficient operation of OECTs, it is imperative that the channel material provides excellent charge/electronic transport while facilitating the penetration and intercalation of electrolyte ions. The simultaneous transport of electronic/ionic charge is referred to as organic mixed ionic-electronic conduction (OMIEC), and the optimization of this parameter has generated new avenues in the structural engineering of CPs. In general, the structures of CPs in OECTs require similar characteristics as that of OFETs, but a key difference is the inclusion of EG_n sidechains to increase the hydrophilicity of the polymer

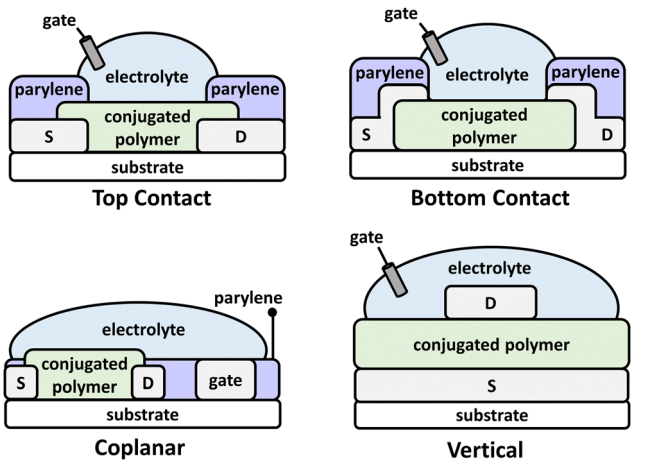

Fig. 7 OECT device architectures including top contact, bottom contact, coplanar, and vertical.

(essential when aqueous electrolytes are used) and to support electrolyte cation transport. Additionally, as with OFETs, the device operational mechanism of OECTs is not directly dependent on the polymer optical absorption; however, many state-of-the-art polymers demonstrate NIR optical absorption due to the preferential arrangement of energy levels, *e.g.* the polymer IP/EA and corresponding optical bandgap. These polymers are most often synthesized *via* Stille polymerization, indicating a need for the introduction of more sustainable polymerization methods. Although Mei *et al.* and Thelakkat *et al.* have demonstrated synthesis of DPP NIR-CPs *via* DArP and their incorporation into OECTs.[144,145] In this review, NIR-CPs incorporated into OECTs include isoindigo (Section 4.1) and diketopyrrolopyrrole analogues (Section 4.2).

4. Donor–acceptor conjugated copolymers with NIR-optical absorption

In this section, copolymers containing isoindigo (IID), diketopyrrolopyrrole (DPP), naphthalene diimide (NDI), fused-ring electron acceptors (FREAs), and cyclopentadithiophene (CDT) and analogues are described. The polymer λ_{max}/E_g, EA/IP, and notable organic electronic device performance are tabulated, and key synthetic steps, functionalization strategies, and aspects synthetic sustainability are indicated when relevant.

4.1 Isoindigo (IID) analogues

IID has remained a prominent component of CPs since its original disclosure by Reynolds *et al.*[146,147] The IID core is highly modular, providing facile access to a variety of structural analogues, and can be prepared in a few number of scalable synthetic steps.[147,148] It has demonstrated utility in a variety of organic electronic applications notably ECDs, OPV, OFETs, and OECTs. IID monomers have also been employed in DArP including flow-synthesis, which avoids polymer batch-to-batch variation and provides large-scale continuous polymer synthesis.[127,149] Polymer structures are provided in Fig. 8 with optical absorption (λ_{max}), optical bandgap (E_g), IP/EA, and device performance metrics tabulated in Table 1. Through extensive structural optimization, such as sidechain engineering and proper pairing of the electron donor repeat unit, excellent charge motilities in OFETs have been achieved (μ_h = 3.62 $cm^2\ V^{-1}\ s^{-1}$) with **P1 (IIDDT-C3)**, which possesses optical absorption at the edge of the NIR wavelength region (λ_{max} = 719 nm and E_g = 1.58 eV).[150] The elegantly designed sidechain of **P1 (IIDDT-C3)** provides a branching site further away from the conjugated polymer backbone allowing for more efficient polymer packing and shorter π–π distances (3.57 Å). Changing the identity of the donor repeat unit to one that is more electron donating, e.g, bis-EDOT, can narrow the bandgap and shift the optical absorption further into the NIR region, such as with **P2 [p(IID-2EDOT)]** which provides a red shift (λ_{max} = 740 nm and E_g = 1.32 eV) and enables NIR optical switching in ECDs [CE (1040 nm) = 433 $cm^2\ C^{-1}$].[151] **P2 [p(IID-2EDOT)]** also provided the shortest bleaching times (t_b) when compared to its bithiophene analogue (8.7 s *versus* 30.5 s, respectively). The Incorporation of EG_n sidechains, such as with **P3 (IG-T)** imparts hydrophilicity essential for OECT operation affording g_m = 0.023 S cm^{-1}, and thiophene is used in this case leading to blue shift in optical absorption relative to P1 (λ_{max} = 712 nm and E_g = 1.57 eV).[152] Inclusion of a vinylene or thienothiophene π-spacer between IID units and the strategic incorporation of heteroatoms enables ambipolar charge transport in OFETs for **P4 (PF_4IVI2T)** and **P5 (PITTI-BT)** (μ_h/μ_e = 1.03/1.82 $cm^2\ V^{-1}\ s^{-1}$ and 3.06/2.81 $cm^2\ V^{-1}\ s^{-1}$) allowing optical absorption to extend further into the NIR wavelength range (E_g = 1.57 and 1.52 eV), respectively.[153,154] For **P4 (PF_4IVI2T)** and **P5 (PITTI-BT)** incorporation of a π-spacer and fluorine substituents provided stronger intermolecular interactions and improved polymer packing, including a preferential edge-on orientation. Additionally, **P5 (PITTI-BT)** was processed using *p*-xylene, which is a more sustainable processing solvent, in place of halogenated solvents.[154]

To alleviate steric hindrance between the phenyl C–H and the lactone carbonyl C–O in the IID core, McCulloch *et al.* developed thienoisoindigo (TIID), which has favourable S–O chalcogen interactions and reduced steric hindrance thereby affording a more conformationally coplanar structure with improved π–π orbital overlap.[155] The polymer **P6 (IGT-BT)** possesses strong NIR optical absorption (λ_{max} = 1035 nm), a very narrow optical bandgap (E_g = 0.92 eV), and balanced ambipolar charge transport properties (μ_h/μ_e = 0.10/0.16 $cm^2\ V^{-1}\ s^{-1}$).[155] Even with phenylene as a repeat unit **[P7 (PTIIP)]**, TIID affords desirable NIR optical absorption (λ_{max} = 872 nm) and narrow optical bandgap (E_g = 1.18 eV), albeit with sacrificed charge transport properties (μ_h = 5×10^{-3} $cm^2\ V^{-1}\ s^{-1}$).[156] A unique approach to improve the sustainability of CP synthesis includes the preparation of **P8 [p(TII-PD)]** by Nozaki *et al.*, which can be prepared *via* acid catalysed condensation between the respective aldehyde and amine functionalized monomers.[157] **P8 [p(TII-PD)]** provides good NIR optical absorption (λ_{max} = 770 nm and E_g = 1.32 eV) with respectable OFET charge mobility ($\mu_h = 1.83 \times 10^{-2}$ $cm^2\ V^{-1}\ s^{-1}$). Characterization of the morphology of microstructure of **P8 [p(TII-PD)]** indicate a fibrous, bundled polymer aggregates with large voids and a bimodal orientation. Notably, **P8 [p(TII-PD)]** can be recycled to its monomers *via* acid catalysed hydrolysis and repolymerized. This demonstrates a unique capability for this polymer, and the imperative task of generating more sustainable polymerization methods should generate renewed interest in poly(azomethines).[167–170]

Another variation of isoindigo includes diazaisoindigo, which incorporates pyridine to alleviate steric hindrance and provide a more coplanar conformation to increase π-conjugation throughout the π-system.[158,161,171] Towards the synthesis of **P9 (PAIID-BT-C3)**, Huang *et al.* demonstrated a targeted approach towards the development of new polymer structures by first using computation to model monomers to ensure desirable torsion angles and coplanarity.[158] **P9 (PAIID-BT-C3)** then afforded broad optical absorption throughout the visible wavelength range and into the NIR region (λ_{max} = 756 nm and E_g = 1.50 eV) with ambipolar charge transport in OFETs (μ_h/μ_e = 0.10/0.16 $cm^2\ V^{-1}\ s^{-1}$).

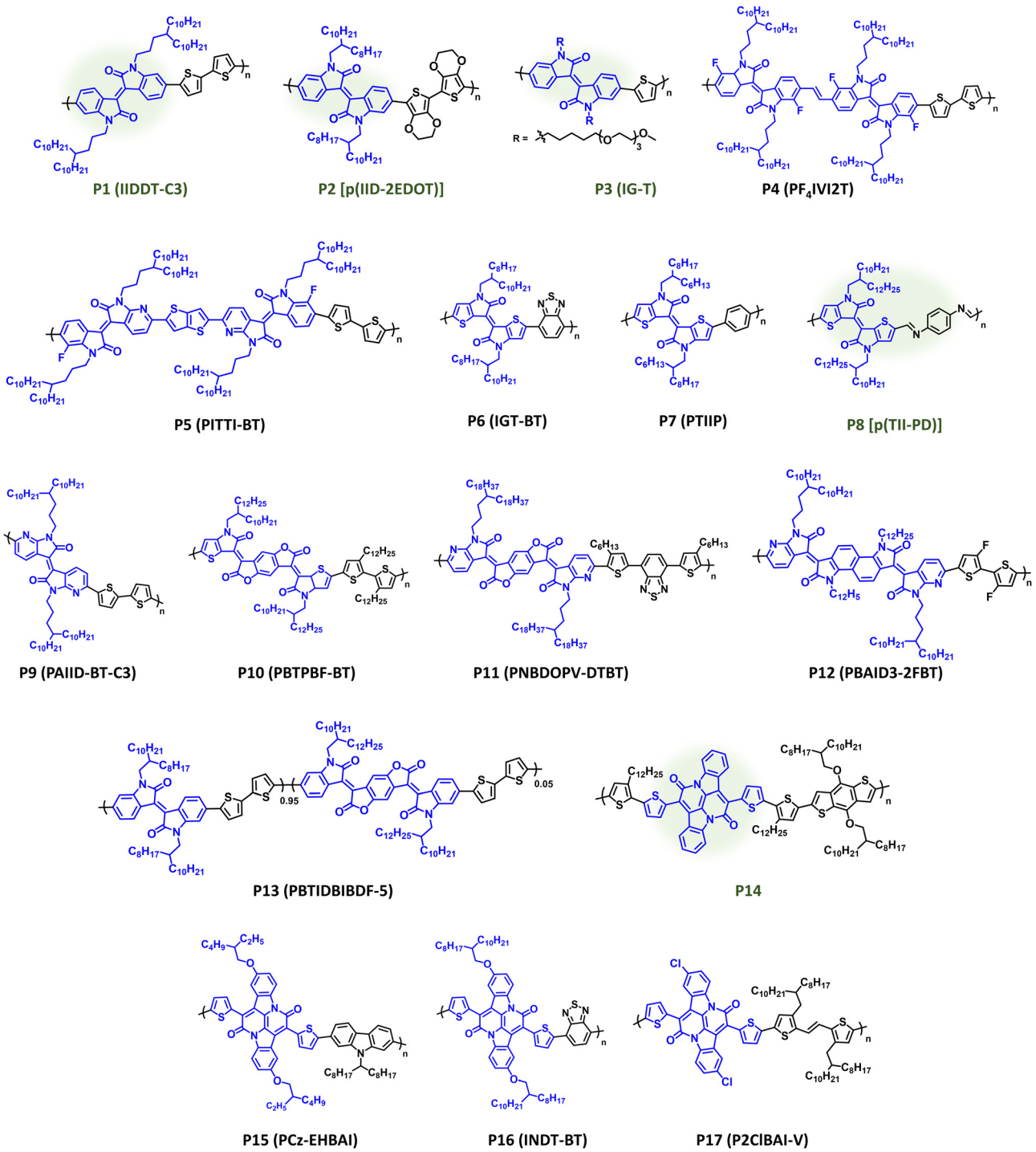

Fig. 8 Select examples of NIR-CPs containing IID, IID analogues, and BAI repeat units. IID analogues repeat units and NIR-CPs with relatively sustainable syntheses are highlighted in green.

Incorporation of the highly electron deficient benzodifurandione (BDO) between lactone units in IID has proven to be an effective strategy to improve charge transport and significantly red shift optical absorption of IID analogues.[136,159,172–175] The TIID analogue **P10 (PBTPBF-BT)** affords strong NIR optical absorption (λ_{max} = 1107 nm and E_g = 0.43 eV), while achieving ambipolar charge transport in OFETs (μ_h/μ_e = 0.34/0.13 cm^2 V^{-1} s^{-1}).[159] The polymer demonstrated robust ambient stability, since it was found that the OFET charge mobilities closely maintained their original values (μ_h/μ_e = 0.34/0.13 cm^2 V^{-1} s^{-1}) when tested under ambient conditions. **P11 (PNBDOPV-DTBT)**, which is an azaisoindigo analogue, provides desirable NIR optical absorption (λ_{max} = 797 nm and E_g = 1.27 eV) with superior OFET charge mobilities (μ_h/μ_e = 5.97/7.07 cm^2 V^{-1} s^{-1}) under ambient testing

Table 1 Tabulated λ_{max}, E_g, ionization potential (IP)/electron affinity (EA), and device performance metrics for the IID and BAI NIR-CPs

Polymer[a]	λ_{max} (nm); E_g[b] (eV)	IP/EA (eV)	Device application[c]	Notable performance metric	Ref.
P1 (IIDDT-C3)	719; 1.58	−5.52/−3.74	OFET (BGTC)	μ_h = 3.62 cm^2 V^{-1} s^{-1}	150
P2 [p(IID-2EDOT)]	740; 1.32	−5.06/−4.05	ECD (vertical)	CE (1040 nm) = 433 cm^2 C^{-1}	151
P3 (IG-T)	712; 1.57	−5.3/−3.8	OECT (top contact)	g_m = 0.023 S cm^{-1}	152
P4 (PF4IVI2T)	728; 1.57	−5.74/−4.17	OFET (TGBC)	μ_h/μ_e = 1.03/1.82 cm^2 V^{-1} s^{-1}	153
P5 (PITTI-BT)	752; 1.52	−5.71/−4.19	OFET (TGBC)	μ_h/μ_e = 3.06/2.81 cm^2 V^{-1} s^{-1}	154
P6 (IGT-BT)	1035; 0.92	−4.86/−3.73	OFET (TGBC)	μ_h/μ_e = 0.10/0.16 cm^2 V^{-1} s^{-1}	155
P7 (PTIIP)	872; 1.18	−4.99/−3.63	OFET (BGBC)	μ_h = 5 × 10^{-3} cm^2 V^{-1} s^{-1}	156
P8 [p(TII-PD)]	770; 1.32	−5.21/−3.89	OFET (BGTC)	μ_h = 1.83 × 10^{-2} cm^2 V^{-1} s^{-1}	157
P9 (PAIID-BT-C3)	756; 1.50	−5.67/−3.64	OFET (BGBC)	μ_h/μ_e = 0.48/0.78 cm^2 V^{-1} s^{-1}	158
P10 (PBTPBF-BT)	1107; 0.43	−5.18/−3.94	OFET (BGTC)	μ_h/μ_e = 0.34/0.13 cm^2 V^{-1} s^{-1}	159
P11 (PNBDOPV-DTBT)	876; 1.26	−5.64/−4.38	OFET (TGBC)	μ_h/μ_e = 5.97/7.07 cm^2 V^{-1} s^{-1}	160
P12 (PBAID3-2FBT)	797; 1.27	−5.17/−3.90	OFET (BGTC)	μ_h/μ_e = 1.68/1.37 cm^2 V^{-1} s^{-1}	161
P13 (PBTIDBIBDF-5)	n.r./1.51	−5.58/−3.74	OPT (BGTC)	R (650 nm) = 128 A W^{-1}	162
P14	783; 1.24	−4.91/−3.63	OFET (BGBC)	μ_h/μ_e = 1.5/0.41 cm^2 V^{-1} s^{-1}	163
P15 (PCz-EHBAI)	692; 1.52	−5.21/−3.57	ECD (vertical)	CE (1100 nm) = 451 cm^2 C^{-1}	164
P16 (INDT-BT)	820; 1.23	−4.97/−3.74	OFET (TGBC)	μ_h/μ_e = 0.52/3.11 cm^2 V^{-1} s^{-1}	165
P17(P2ClBAI-V)	897; 1.04	−5.32/−3.70	OFET (TGBC)	μ_h/μ_e = 4.04/1.06 cm^2 V^{-1} s^{-1}	166

[a] Abbreviation in parentheses indicates common name. [b] Estimated in all cases using λ_{onset} where optical E_g = 1240/λ_{onset}. [c] Device architecture is indicated in parentheses (see Section 3). n.r. = not reported.

conditions.[160] **P11 (PNBDOPV-DTBT)** was then incorporated into a complementary inverter on a flexible PET substrate yielding a gain of 148. Lastly, **P12 (PBAID3-2FBT)**, which incorporates a naphthalene bis-isatin flanked by azaisoindigo analogues additionally affords ambipolar charge transport in OFETs (μ_h/μ_e = 1.68/1.37 cm^2 V^{-1} s^{-1}) with a slight blue shift relative to **P10**/**P11** (λ_{max} = 876 nm and E_g = 1.26 eV).[161] Following storage of **P12** OFET devices for 173 days, the charge mobilities were maintained relatively close to their initial values (μ_h/μ_e = 0.428/0.276 cm^2 V^{-1} s^{-1}) indicating excellent stability. **P13 (PBTIDBIBDF-5)**, is a semi-random copolymer incorporating isoindigo and BDO acceptor repeat units where the composition and percentage of BDO is finely tuned to increase NIR optical absorption (E_g = 1.51 eV) while maintaining suitable charge transport properties for use in OPTs.[162] A responsivity (650 nm) of 128 A W^{-1} was obtained from OPTs incorporating **P13** blended with 1% PBA. Flexible OPTs using PET as the substrate were found to provide R (650 nm) of 180 mA W^{-1}. As detailed here, the incorporation of benzodifuradione and its structural analogues is a promising strategy to impart excellent hole and electron charge transport properties with ambient stability and strong optical absorption in the NIR. Additionally, McCulloch *et al.* have demonstrated naphthalene bis-isatin containing polymers can be prepared *via* aldol condensation polymerization, which provides a more sustainable polymerization methodology.[136]

Bay annulated indigo (BAI) or indolonapthyridine can be synthesized directly from the naturally occurring dye, indigo, *via* a single, scalable condensation step to afford the π-extended fused ring structure.[163,165,176] The fused ring structure and structural tunability of BAI impart excellent optical absorption and charge transport properties in the corresponding polymers (**P14–P17**). Lie *et al.* disclosed the initial synthesis of BAI towards the preparation of **P14**, which provided optical absorption on the edge of the NIR wavelength range (λ_{max} = 783 nm and E_g = 1.24 eV) and desirable ambipolar charge transport in OFETs (μ_h/μ_e = 1.5/0.41 cm^2 V^{-1} s^{-1}).[163] This work was followed up with the introduction of sidechains onto the BAI core and copolymerization with carbazole to yield **P15 (PCz-EHBAI)**, which provided ECDs with remarkably stable optical switching (>7500 cycles) at NIR wavelengths [CE (1100 nm) = 451 cm^2 C^{-1}].[164] Suzuki–Miyaura polymerization of alkylated BAI with benzothiadiazole afforded **P16 (INDT-BT)**, which provides strong NIR optical absorption (λ_{max} = 820 nm and E_g = 1.23 eV) and notable ambipolar charge transport in OFETs (μ_h/μ_e = 0.52/3.11 cm^2 V^{-1} s^{-1}).[165] The strategic incorporation of heteroatoms on BAI and an alkylated TVT comonomer affords **P17 (P2CIBAI-V)**, which provided a significant red shift in the optical absorption (λ_{max} = 897 nm and E_g = 1.04 eV) with excellent OFET charge mobilities (μ_h/μ_e = 4.04/1.06 cm^2 V^{-1} s^{-1}).[166] Microstructural characterization of **P17 (P2CIBAI-V)** using GIWAXS indicated a bimodal orientation and excellent π–π stacking with distances of 3.54 Å. Overall, BAI is a promising candidate for numerous device applications in organic electronics, and its inherent sustainability, due to indigo serving as a naturally sourced monomer feedstock, and ease of synthesis relative to other acceptor repeat units makes it a valuable target for future work.

4.2 Diketopyrrolopyrrole (DPP) analogues

DPP is one of the most prevalent acceptor repeat units in CPs given its notable utility in OPV, OFETs, and OECTs following disclosure by Janssen *et al.* of high-performance DPP donor polymers for fullerene solar cells.[177–181] As with IID, DPP possesses high structural tunability *via* facile modification of the pendant aryl groups and alkyl substituents, relative ease of synthesis, and desirable optical and electronic properties suitable for a wide range of organic electronic device applications.[182] It is notable that many DPP containing CPs have been synthesized *via* DArP, which significantly improves the overall sustainability of the CP synthesis.[129,130,144,145,183–186] DPP containing NIR-CPs and analogues described here are provided in Fig. 9 with optical absorption (λ_{max}) and bandgap (E_g), IP/EA, and device performance metrics tabulated in Table 2. Pairing DPP with the π-extended donor TVT affords **P18 (PDVT-10)**, which is a well-studied NIR-CP

(λ_{max} = 783 nm and E_g = 1.40 eV) exhibiting state-of-the-art hole mobilities under ambient testing conditions (μ_h = 11.0 $cm^2 V^{-1} s^{-1}$).[187,188] **P18 (PDVT-10)** has also been incorporated into flexible and stretchable OFETs, electronic skin, and photodetectors demonstrating the broad utility of this NIR-CP.[187–190] Incorporation of a more electron donating repeat unit, EDOT, provides **P19 (DPP-E)**, which demonstrates a significant red shift in the optical absorption relative to **P18 (PDVT-10)** (λ_{max} = 914 nm and E_g = 1.19 eV) and imparts electrochemical stability rendering the polymer suitable for use in NIR-ECDs [CE (1180 nm) = 901 $cm^2 C^{-1}$].[191–193] Replacement of the alkyl substituents on **P19 (DPP-E)** with EG_n side-chains to improve electrolyte uptake provides **P20 (gDPP-E)**, which affords improved ΔT% metrics in NIR-ECDs relative to **P19** (24.2% *versus* 18.8%, respectively) and has demonstrated utility in OECTs.[92,194] Copolymerization of glycolated DPP with EG_n functionalized bithiophene yields **P21 (gDPP-g2T)**,which further red shifts the optical absorption (λ_{max} = 834 nm and

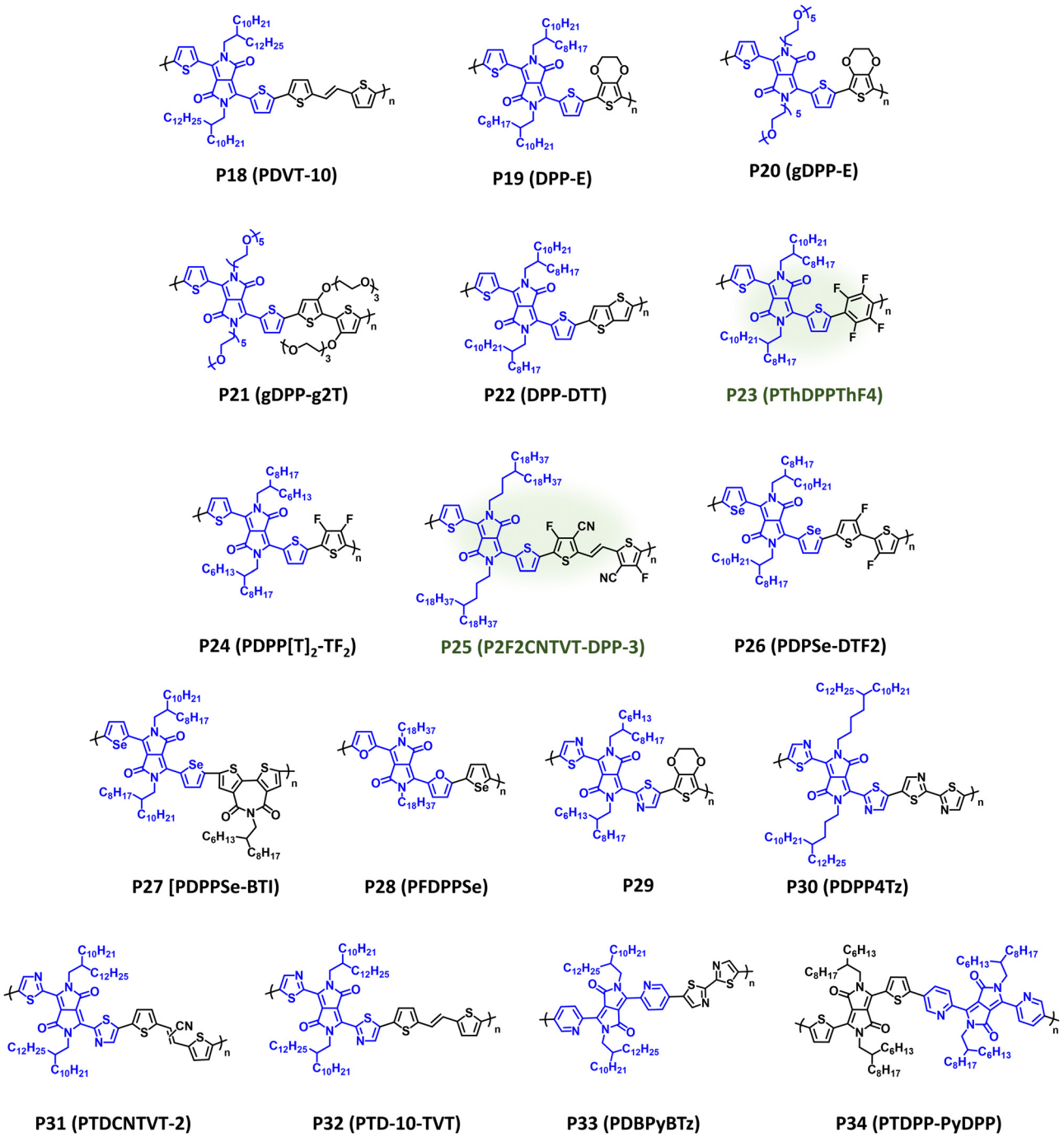

Fig. 9 Select examples of NIR-CPs containing DPP analogues. DPP NIR-CPs with relatively sustainable syntheses are highlighted in green.

Table 2 Tabulated λ_{max}, E_g, ionization potential (IP)/electron affinity (EA), and device performance metrics for DPP NIR-CPs

Polymer[a]	λ_{max} (nm); E_g[b] (eV)	IP/EA (eV)	Device application[c]	Notable performance metric	Ref.
P18 (PDVT-10)	783; 1.40	−5.28; −3.60	OFET (BGTC)	μ_h = 11.0 cm^2 V^{-1} s^{-1}	187
P19 (DPP-E)	834; 1.19	−5.04/−3.85	ECD (vertical)	CE (1180 nm) = 901 cm^2 C^{-1}	192
P20 (gDPP-E)	853; 1.12	−4.60/n.r.	ECD (vertical)	ΔT% (853 nm) = 24.2%	92
P21 (gDPP-g2T)	914; 1.08	n.r.	OECT (vertical)	$g_{m,A}$ = 226.1 μS μm^2	93
P22 (DPP-DTT)	818; 1.36	−5.22/−3.86	OPT (BGTC)	R (850 nm) = 246 A W^{-1}	196
P23 (PThDPPThF4)	775; 1.45	−4.65/−3.20	OFET (TGBC)	μ_e = 0.44 cm^2 V^{-1} s^{-1}	183
P24 (PDPP[T]2-TF2)	836; 1.3	−5.91/−3.70	OFET (BGBC)	μ_h/μ_e = 0.22/0.19 cm^2 V^{-1} s^{-1}	197
P25 (P2F2CNTVT-DPP-3)	864; 1.32	−5.43/−3.67	OFET (TGBC)	μ_e = 1.61 cm^2 V^{-1} s^{-1}	184
P26 (PDPSe-DTF2)	836; 1.33	−5.30/−3.97	OFET (BGTC)	μ_h/μ_e = 0.16/0.006 cm^2 V^{-1} s^{-1}	198
P27 (PDPPSe-BTI)	804; 1.32	−5.38/−3.51	OFET (BGTC)	μ_h/μ_e = 0.025/0.154 cm^2 V^{-1} s^{-1}	199
P28 (PFDPPSe)	832, 1.34	−5.5/−3.8	OPV (inverted)	PCE = 6.16%	200
P29	820; 1.30	−5.10/−3.61	ECD (vertical)	t_b/t_c (760 nm) = 6.9/0.5 s	191
P30 (PDPP4Tz)	715; 1.34	−5.71/−3.9	OFET (BGBC)	μ_e = 0.067 cm^2 V^{-1} s^{-1}	201
P31 (PTDCNTVT-2)	776; 1.39	−5.80/−3.72	OFET (TGBC)	μ_h/μ_e = 1.28/0.97 cm^2 V^{-1} s^{-1}	202
P32 (PTD-10-TVT)	770; 1.47	−5.40/−3.64	OFET (BGBC)	μ_h/μ_e = 0.17/0.0097 cm^2 V^{-1} s^{-1}	203
P33 (PDBPyBTz)	656; 1.47	−5.45/−3.84	OFET (BGBC)	μ_e = 0.023 cm^2 V^{-1} s^{-1}	204
P34 (PTDPP-PyDPP)	792; 1.43	−5.96/−4.00	OPV (inverted)	PCE = 0.2%	205

[a] Abbreviation in parentheses indicates common name. [b] Estimated in all cases using λ_{onset} where optical E_g = 1240/λ_{onset}. [c] Device architecture is indicated in parentheses (see Section 3). n.r. = not reported.

E_g = 1.08 eV), and it affords notable performance metrics in OECTs ($g_{m,A}$ = 226.1 μS μm^2) where the incorporation of EG$_n$ sidechains increases hydrophilicity and electrolyte exchange.[93] **P22 (DPP-DTT)** incorporates the fused thiophene donor unit thieno[3,2-*b*]thiophene (TT) providing broad NIR optical absorption with λ_{max}/E_g of 818 nm/1.36 eV.[195,196] Blends of **P22**:polystyrene yielded nanowire networks for efficient charge transport, and coupled with the strong NIR optical absorption an R (850 nm) = 246 A W^{-1} was achieved.[196]

While DPP is typically used for hole transport materials or p-type CPs, copolymerization with fluorinated donor units tunes the EA providing CPs with energy levels suitable for electron transport, while retaining NIR optical absorption with **P23–P26** as examples. **P23 (PThDPPThF4)**, which was synthesized *via* DArP and affords desirable electron mobilities in OFETs (μ_e = 0.44 cm^2 V^{-1} s^{-1}) and broad optical absorption extending into the NIR (λ_{max} = 775 nm and E_g = 1.45 eV).[183] Incorporation of a fluorinated thiophene donor provides a substantial red shift in the optical absorption for **P25 (PDPP[T]$_2$-TF$_2$)** (λ_{max} = 836 nm and E_g = 1.3 eV) and imparts ambipolar charge transport characteristics in OFETs (μ_h/μ_e = 0.22/0.19 cm^2 V^{-1} s^{-1}).[197] These excellent charge transport properties were attributed to the improved crystallinity and intermolecular π–π interactions imparted through incorporation of the perfluorothiophene comonomer. **P25 (P2F2CNTVT-DPP-3)**, which was synthesized *via* DArP, demonstrated strategic sidechain engineering and functionalization of the TVT donor with nitrile and fluorine substituents affording excellent OFET electron mobility (μ_e = 1.61 cm^2 V^{-1} s^{-1}) with a λ_{max}/E_g of 864 nm/1.32 eV.[184] The extensive functionalization of **P25 (P2F2CNTVT-DPP-3)** is a testament to the functional group tolerance of DArP, and a masterful demonstration of structural engineering to maximize crystalline domains, control polymer chain orientation, and afford a well-ordered fibril morphology.

As previously noted, the incorporation of selenophene and other chalcogenophenes provides another handle for tailoring the optical and electronic properties of DPP based NIR-CPs *via* modification of the orbital overlap in the π-system and tuning the intermolecular interactions and self-assembly between polymers and chalcogen centers.[60,200,206–209] **P26 (PDPSe-DTF2)** and **P27 (PDPPSe-BTI)** incorporate the selenophenyl aryl substituent in place of the 2-thienyl, and both possess similar optical bandgaps (λ_{max} = 836 nm and E_g = 1.33 eV and λ_{max} = 804 nm and E_g = 1.32 eV) with desirable OFET charge transport characteristics (μ_h/μ_e = 0.16/0.006 cm^2 V^{-1} s^{-1} and 0.025/0.154 cm^2 V^{-1} s^{-1}), respectively.[198,199] **P28 (PFDPPSe)** provides strong NIR-optical absorption (λ_{max} = 832 nm and E_g = 1.34 eV) suitable for harvesting NIR wavelengths in OPV applications, and it afforded a champion PCE of 6.16% when blended with PC$_{71}$BM and with a notable active layer thickness of 210 nm.[200]

As with IID, the incorporation of azaheterocycles, such as 2-thiazolyl,[183,191,201,204,210] 2-pyridiyl,[197,198,204,205] and 2-pyrazinyl,[211,212] into the DPP scaffold can be readily accomplished with **P29–P34** provided as examples. **P29**, which is the 2-thiazolyl analogue of **P29**, demonstrates a blue shift in optical absorption relative to **P29** (λ_{max} = 820 nm and E_g = 1.30 eV) and NIR optical switching when incorporated into ECDs [t_b/t_c (760 nm) = 6.9/0.5 s].[191] Sidechain engineering and strategic pairing with a bithiazole comonomer afforded the n-channel NIR-CP **P30 (PDPP4Tz)**, which possesses broad optical absorption extending throughout the visible wavelength range and into the NIR (λ_{max} = 715 nm and E_g = 1.34 eV) and efficient OFET electron mobilities (μ_e = 0.067 cm^2 V^{-1} s^{-1}).[201] It is worth noting **P30 (PDPP4Tz)** was processed using blade coating using the less toxic and more sustainable solvent *p*-xylene, and the devices demonstrated excellent ambient stability for over 100 days. Comparing polymers **P31 (PTDCNTVT-2)** and **P32 (PTD-10-TVT)**, which contain a nitrile functionalized TVT and unfunctionalized TVT, incorporation of the nitrile provides a slight red shift in the optical absorption (λ_{max} = 776 nm and E_g = 1.39 eV *versus* λ_{max} = 770 nm and E_g = 1.47 eV) and a

significant increase in OFET charge mobilities (μ_h/μ_e = 1.28/0.97 $cm^2\ V^{-1}\ s^{-1}$ *versus* μ_h/μ_e = 0.17/0.0097 $cm^2\ V^{-1}\ s^{-1}$).[202] Notably, OFET characterization for **P31 (PTDCNTVT-2)** occurred under ambient conditions, and inverters incorporating **P31 (PTDCNTVT-2)** provided an impressive gain of 168.[202,203] Lastly, incorporation of the 2-pyridyl aryl group in DPP is depicted with the polymers **P33 (PDBPyBTz)** and **P34 (PTDPP-PyDPP)**, which show a strong dependence of the comonomer identity on the polymer optical and electronic properties.[204] Specifically, **P33 (PDBPyBTz)** provides optical absorption extending throughout the visible spectrum and into the NIR wavelength region (λ_{max} = 656 nm and E_g = 1.47 eV) and achieves good OFET electron mobility (μ_e = 0.023 $cm^2\ V^{-1}\ s^{-1}$).[204,205] **P34 (PDTDPP-PyDPP)** provides strong NIR optical absorption (λ_{max} = 792 nm and E_g = 1.43 eV) but affords a only modest PCE of 0.2% in all-polymer solar cells (APSCs) when paired with donor polymer **PTB7-Th** (Fig. 5), due to an unfavourable energy level alignment, which indicates a potential area for future structural optimization.[205]

Overall, DPP and its analogues afford NIR-CPs with numerous handles for structural modification and functionalization, compatibility with more sustainable polymerization methods, such as DArP, and processing conditions, such as the use non-halogenated solvents, excellent overall stability, and robust mechanical properties. Thus, it is foreseeable that DPP based polymers will continue to provide a substantial contribution towards the further advancement of NIR-CPs in organic electronics.

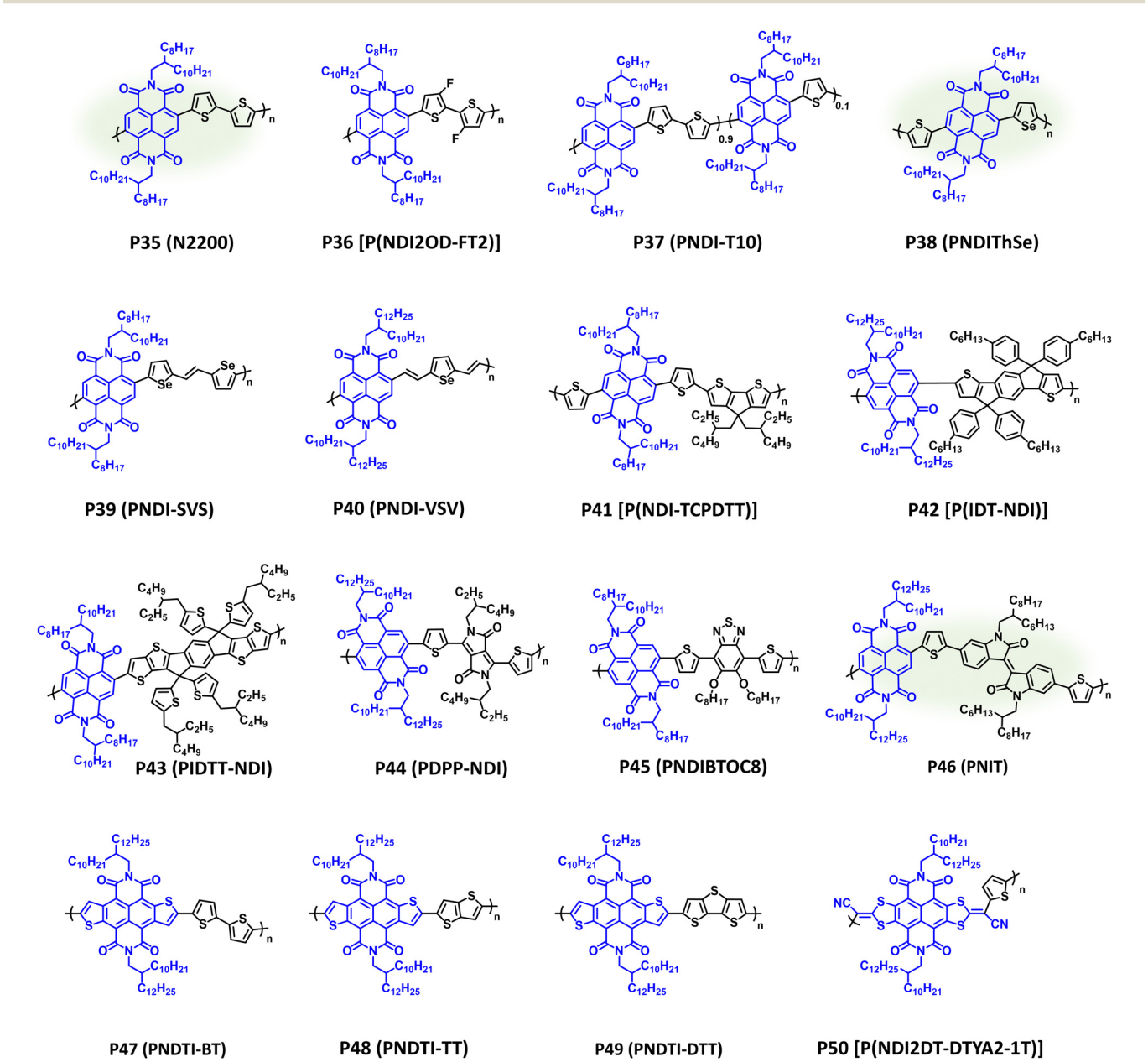

Fig. 10 Select examples of NIR-CPs containing repeat units of NDI and analogues. NDI NIR-CPs with relatively sustainable syntheses are highlighted in green.

4.3 Naphthalene diimide (NDI) analogues

Following independent disclosure by Facchetti *et al.* and Watson *et al.*, NDI CPs have provided exceptional electron transport properties with robust ambient stability and extensive use in OPV, OFETs, and OECTs.[182,213–215] Although not as modular or structurally tuneable as IID and DPP, numerous NIR-CPs containing NDI have been reported with select examples provided in Fig. 10 and λ_{max}/E_g, IP/EA, and device performance metrics tabulated in Table 3. The polymer **P35 (N2200)** achieved remarkable initial OFET electron mobilities of 0.85 $cm^2\ V^{-1}\ s^{-1}$ when processed from dichlorobenzene and 0.45 $cm^2\ V^{-1}\ s^{-1}$ when processed from xylenes.[216] By controlling the polymer chain orientational alignment and self-assembly the electron mobility of **P35 (N2200)** was increased to 6.4 $cm^2\ V^{-1}\ s^{-1}$ when processed from mesitylene solutions.[217] In APSCs, **P35 (N2200)** provides complimentary NIR optical absorption (λ_{max} = 700 nm and E_g = 1.50 eV) to many medium or wide bandgap donor polymers, and it has afforded PCEs of 11% after being blended with the donor polymer **PTzBI-Si** (Fig. 5) and processed from the sustainable solvent cyclopentyl methyl ether (CPME).[88] Additionally, **P35 (N2200)** has been synthesized *via* DArP with extensive optimization of the polymerization conditions and defect pathways provided by Sommer *et al.*[218,219] Thus, **P35 (N2200)** is exemplary n-type polymer capable of being processed using sustainable solvents and synthesized using more sustainable polymerization conditions; however, due to the lack of structural tunability and steric hindrance imparted by the naphthalene core, structural engineering is often limited to sidechain modification or pairing with a different comonomer. Examples of NDI NIR-CPs with different donor repeat units other than bithiophene are provided with polymers **P36–P42. P36 [P(NDI2OD-FT2)]** includes fluorine substitution on the bithiophene donor unit, which slightly widened the bandgap and provided a pronounced blue shift in optical absorption (λ_{max} = 630 nm and E_g = 1.59 eV).[220] Blending with **PTB7-Th** afforded a champion PCE of 6.71% in APSCs. **P37 (PNDI-T10)** is a semi-random copolymer where two different donor comonomers (thiophene and bithiophene) were copolymerized with the NDI acceptor. 10% incorporation of thiophene afforded the optimal polymer composition by finely tuning the polymer microstructure and facilitating improved donor–acceptor polymer miscibility in APSCs.[221] Thus, a PCE of 9.0% was achieved in ternary APSCs when **P37 (PNDI-T10)** was blended with the donor polymers **PTB7-Th** and **PBDTTS-FTAZ** (Fig. 5).[222] As with DPP, incorporation of different chalcogenophenes, such as selenophene, is another common strategy for structurally engineering NDI based NIR-CPs. Examples of this include **P38–P40**, which have been incorporated into OFETs and APSCs and provide comparable optical absorption to **P35 (N2200)**.[128,223,224] Notably, **P38 (PNDIThSe)** was synthesized using the more sustainable Zn-anionic radical polymerization, which was first reported by Kiriy *et al.* for the synthesis of **P35 (N2200)**.[128,225,226] As with **P37 (PNDI-T10)**, the asymmetric structure of **P38 (PNDIThSe)** helps suppress crystallization and improves miscibility between the donor and acceptor polymers in APSCs.[128] This provides a PCE of 6.41% when blended with **PBDB-T** (Fig. 5). **P39 (PNDI-SVS)**, which incorporates a selenophene TVT analogue as the donor unit, provides a red shift in optical absorption and narrower bandgap (λ_{max} = 748 nm and E_g = 1.31 eV) relative to **P35 (N2200)**.[223] **P39 (PNDI-SVS)** possesses an EA of −3.98 eV, which affords an impressive OFET electron mobility of 2.4 $cm^2\ V^{-1}\ s^{-1}$, and demonstrates excellent stability when subjected to constant biasing for 3 h under ambient conditions with only a 3% loss in performance metrics. **P40 (PNDI-VSV)** shows a unique functionalization strategy with the incorporation of two vinyl π-spacers attached to a selenophene donor unit.[224] Relative to **P39 (PNDI-SVS)**, **P40 (PNDI-VSV)** shows a reduction in crystal coherence lengths and a preferential face-on orientation *via* GIWAXS measurements, where **P39 (PNDI-SVS)** provides a bimodal orientation containing crystalline domains with face-on and edge-on orientation, which may contribute to the lower electron mobility (μ_e = 0.7 $cm^2\ V^{-1}\ s^{-1}$) of **P40 (PNDI-VSV)**. Notably, **P40 (PNDI-VSV)** was synthesized *via* Suzuki–Miyaura polymerization.

The polymers **P41 [P(NDI-TCPDTT)]** and **P42 [P(IDT-NDI)]** provide examples of NDI based NIR-CPs incorporating fused ring donors, such as CDT and indacenodithiophene (IDT),

Table 3 Tabulated λ_{max}, E_g, ionization potential (IP)/electron affinity (EA), and device performance metrics for NDI NIR-CPs

Polymer[a]	λ_{max} (nm); E_g[b] (eV)	IP/EA (eV)	Device application[c]	Notable performance metric	Ref.
P35 (N2200)	700; 1.50	−5.94/−3.80	OPV (conventional)	PCE = 11.0%	88
P36 [P(NDI2OD-FT2)]	630; 1.59	−5.50/−3.91	OPV (inverted)	PCE = 6.71%	220
P37 (PNDI-T10)	694; 1.55	−6.36/−4.05	OPV (conventional)	PCE = 9.0%	222
P38 (PNDIThSe)	697; 1.50	−5.85/−3.81	OPV (conventional)	PCE = 6.41%	128
P39 (PNDI-SVS)	748; 1.31	−5.29/−3.98	OFET (TGBC)	μ_e = 2.4 $cm^2\ V^{-1}\ s^{-1}$	223
P40 (PNDI-VSV)	714; 1.49	−5.46/−4.06	OFET (TGBC)	μ_e = 0.70 $cm^2\ V^{-1}\ s^{-1}$	224
P41 [P(NDI-TCPDTT)]	830; 1.25	−5.35/−4.15	OPV (conventional)	PCE = 1.1%	227
P42 [P(IDT-NDI)]	730; 1.51	−5.75/−3.84	OPV (conventional)	PCE = 5.33%	228
P43 (PIDTT-NDI)	n.r.; 1.48	−5.69/−4.21	OPT (BGTC)	R (754 nm) = 8.42 $mA\ W^{-1}$	229
P44 (PDPP-NDI)	910; 1.03	−5.46/−3.97	OFET (BGTC)	μ_e = 0.0378 $cm^2\ V^{-1}\ s^{-1}$	230
P45 (PNDIBTOC8)	680; 1.46	−5.82/−3.72	OPV (conventional)	PCE = 3.14%	231
P46 (PNIT)	697; 1.59	−5.94/−3.99	OPV (conventional)	PCE = 5.32%	127
P47 (PNDTI-BT)	800; 1.2	−5.6/−4.4	OFET (BGTC)	μ_h/μ_e = 0.10/0.27 $cm^2\ V^{-1}\ s^{-1}$	232
P48 (PNDTI-TT)	n.r.; 1.3	−5.7/−4.1	OFET (BGTC)	μ_h/μ_e = 0.046/0.26 $cm^2\ V^{-1}\ s^{-1}$	232
P49 (PNDTI-DTT)	833; 1.3	−5.6/−4.0	OPV (conventional)	PCE = 3.2%	233
P50 [P(NDI2DT-DTYA2-1T)]	918; 1.25	−5.82/−4.25	OFET (BGBC)	μ_e = 0.38 $cm^2\ V^{-1}\ s^{-1}$	234

[a] Abbreviation in parentheses indicates common name. [b] Estimated in all cases using λ_{onset} where optical $E_g = 1240/\lambda_{onset}$. [c] Device architecture is indicated in parentheses (see Section 3). n.r. = not reported.

respectively.[227,228] **P41 [P(NDI-TCPDTT)]** possesses strong NIR optical absorption (λ_{max} = 830 nm and E_g = 1.25 eV) and when blended with the donor polymer **P3HT** (Fig. 5) affords a modest PCE of 1.1%. However, it should be noted the APSC was fabricated using tetralin as the processing solvent with an active layer thickness of 410 nm. **P42 [P(IDT-NDI)]** provides a red shift relative **P35 (N2200)** (λ_{max} = 730 nm and E_g = 1.51 eV), and when blended with donor polymer **J51** (Fig. 5) in APSCs a champion PCE of 5.33% is obtained.[228] This improved PCE compared to **P42 [P(IDT-NDI)]** with **J50** (PCE = 4.12%) or **PTB7-Th** (PCE =3.63%) was ascribed to a more complimentary optical absorption between the donor/acceptor polymers and a suitable offset in energy levels (IP/EA) to facilitate charge transfer. **P43 (PIDTT-NDI)** contains a π-extended indacenodithienothiophene donor unit affording a narrower bandgap compared to **P42 [P(IDT-NDI)]** (E_g = 1.48 eV).[229] **P43 (PIDTT-NDI)** was then incorporated into OPTs providing an R (754 nm) = 8.42 mA W^{-1}, and it retained suitable responsivity metrics in flexible OPTs utilizing PEN substrates (R = 3.75 mA W^{-1}).

Copolymerization with another acceptor unit is also an effective strategy to tune the optical and electronic properties of NDI containing NIR-CPs with polymers **P44–P46** as examples.[127,230,231] Notably, **P45 (PNDIBTOC8)** and **P46 (PNIT)**,-which was synthesized using DArP, were both used as acceptor polymers in APSCs with **P46 (PNIT)** providing a red shift in optical absorption (λ_{max} = 697 nm) but wider optical bandgap (E_g = 1.59 eV) relative to **P45 (PNDIBTOC8)** (λ_{max} = 680 nm and E_g = 1.46 eV). When blended with the donor polymer **PBDB-T**, **P46 (PNIT)** affords a maximum PCE of 5.32%.[127] **P45 (PNDIBTOC8)** afforded a comparable PCE of 3.14% when blended with the donor polymer **PBDTTT-C-T** (Fig. 5) in APSCs.[231]

Although there are limited strategies for further functionalization of NDI to modify the optical and electronic properties, Takimiya *et al.* discovered an elegant approach for extension of the π-system yielding naphthodithiophene diimide (NDTI), which is depicted with polymers **P47–P49**.[232,235] NDTI can be synthesized in only two steps from the dibrominated NDI precursor. **P47 (PNDTI-BT)** provides broad optical absorption extending throughout the visible wavelength range deep into the NIR (λ_{max} = 800 nm and E_g = 1.2 eV). Notably, the polymer also affords ambipolar charge transport in OFETs μ_h/μ_e = 0.10/0.27 cm^2 V^{-1} s^{-1}, and shows good ambient stability with the device measurements proceeding in air.[232] **P49 (PNDTI-DTT)** provides a red shift in optical absorption relative to **P47 (PNDTI-BT)** (λ_{max} = 833 nm) with a slight increase in optical bandgap (E_g = 1.3 eV), and provided a respectable PCE of 3.2% in APSCs when blended with **PTB7**.[233] Another example of ring extension with NDI is shown with the polymer **P50 [P(NDI2DT-DTYA2-1T)]**.[234] **P50 [P(NDI2DT-DTYA2-1T)]** provides a narrow optical absorption band almost exclusively in the NIR wavelength region (λ_{max} = 918 nm and E_g = 1.25 eV). Additionally, despite having an amorphous morphology **P50 [P(NDI2DT-DTYA2-1T)]** provides an impressive electron mobility (μ_e = 0.38 cm^2 V^{-1} s^{-1}).

Overall, NIR-CPs incorporating NDI and its analogues afford superb electron mobilities, ambient stability, and broad utility across the field of organic electronics. While there is limited capability with altering the structure of NDI relative to IID or DPP, creative strategies, such as the π-extension and ring fusion with PNDTI, indicate new opportunities for further development and functionalization.

4.4 Benzothiadiazole (BT) analogues

Since disclosure by Meijer *et al.*, benzothiadiazole has afforded numerous state-of-the-art p-type and n-type CPs with prominent utility in OPV and OFET devices.[236–238] As previously discussed, the BT core offers a variety of options for functionalization and derivatization *via* heteroatom substitution, π-extension, and fused ring systems with relevant NIR-CPs (**P51–P67**) provided in Fig. 11 and λ_{max}/E_g, IP/EA, and device performance metrics tabulated in Table 4.

DPP and BT copolymers (**P51–P54** in Table 4) have been shown to provide broad NIR optical absorption and ambipolar charge transport characteristics in OFETs. Specifically, **P51 (PDPP-TBT)** affords strong NIR optical absorption (λ_{max} = 915 nm) with a narrow optical bandgap (E_g = 1.2 eV), and provides balanced ambipolar charge transport (μ_h/μ_e = 0.35/0.40 cm^2 V^{-1} s^{-1}) and a gain of 35 when incorporated into inverters.[239,253] **P51 (PDPP-TBT)** was synthesized using Suzuki–Miyaura polymerization avoiding the toxicity associated with the alkyl-tin residues of Stille polymerization. Additionally, the excellent NIR optical absorption of **P51** makes it suitable for OPTs affording R (935 nm) = 34.78 mA W^{-1}.[254] **P52 (PDPP-FBT)** and **P53 (PDPP-VBBT)** provide examples of heteroatom substitution and π-extension using the **P51 (PDPP-TBT)** scaffold, respectively. **P52 (PDPP-FBT)** demonstrates a blue shift in optical absorption (λ_{max} = 816 nm) relative to **P51 (PDPP-TBT)** and comparable charge mobilities (μ_h/μ_e = 0.21/0.42 cm^2 V^{-1} s^{-1}), albeit with an improved electron mobility.[240] Additionally, **P52 (PDPP-FBT)** adopts a preferential edge-on orientation with π–π distances (3.8 Å) suitable for efficient charge transport in OFETs. In comparison, **P53 (PDPP-VBBT)**, which incorporates a vinylene π-spacer, demonstrates a blue shift relative to **P51** and **P52** (λ_{max} = 918 nm and E_g = 1.25 eV) and provides comparable ambipolar charge transport mobilities (μ_h/μ_e = 0.20/0.15 cm^2 V^{-1} s^{-1}).[241] **P54** incorporates BT with a π-extended fused ring DPP derivative as a second acceptor repeat unit affording strong NIR optical absorption (λ_{max}/E_g = 829 nm/1.27 eV).[242] When blended with $PC_{71}BM$ in OPTs, **P54** provides an R (850 nm) = 118 A W^{-1} with improved photoresponsivity at lower light intensities (1.8 μW cm^{-2}). This trend in responsivity is attributed to a desirable morphology/microstructure for the **P54**/$PC_{71}BM$ blends.

In addition to fluorination, cyanation is another effective strategy to tune the EA of benzothiadiazole CPs to facilitate electron transport with polymers **P55 [P(Ge-DTDCNBT)]** and **P56 (DCNBT-TPC)** as examples.[58,243] **P55 [P(Ge-DTDCNBT)]** affords broad NIR optical absorption (λ_{max} = 754 nm and E_g = 1.27 eV) and demonstrates good electron transport (μ_e = 2.8 × 10^{-3} cm^2 V^{-1} s^{-1}).[58] By pairing with a strategically designed fused-ring donor unit, **P56 (DCNBT-TPC)** affords a substantial red shift in optical absorption (λ_{max} = 841 nm and E_g = 1.38 eV) relative to **P55 [P(Ge-DTDCNBT)]**. This provides

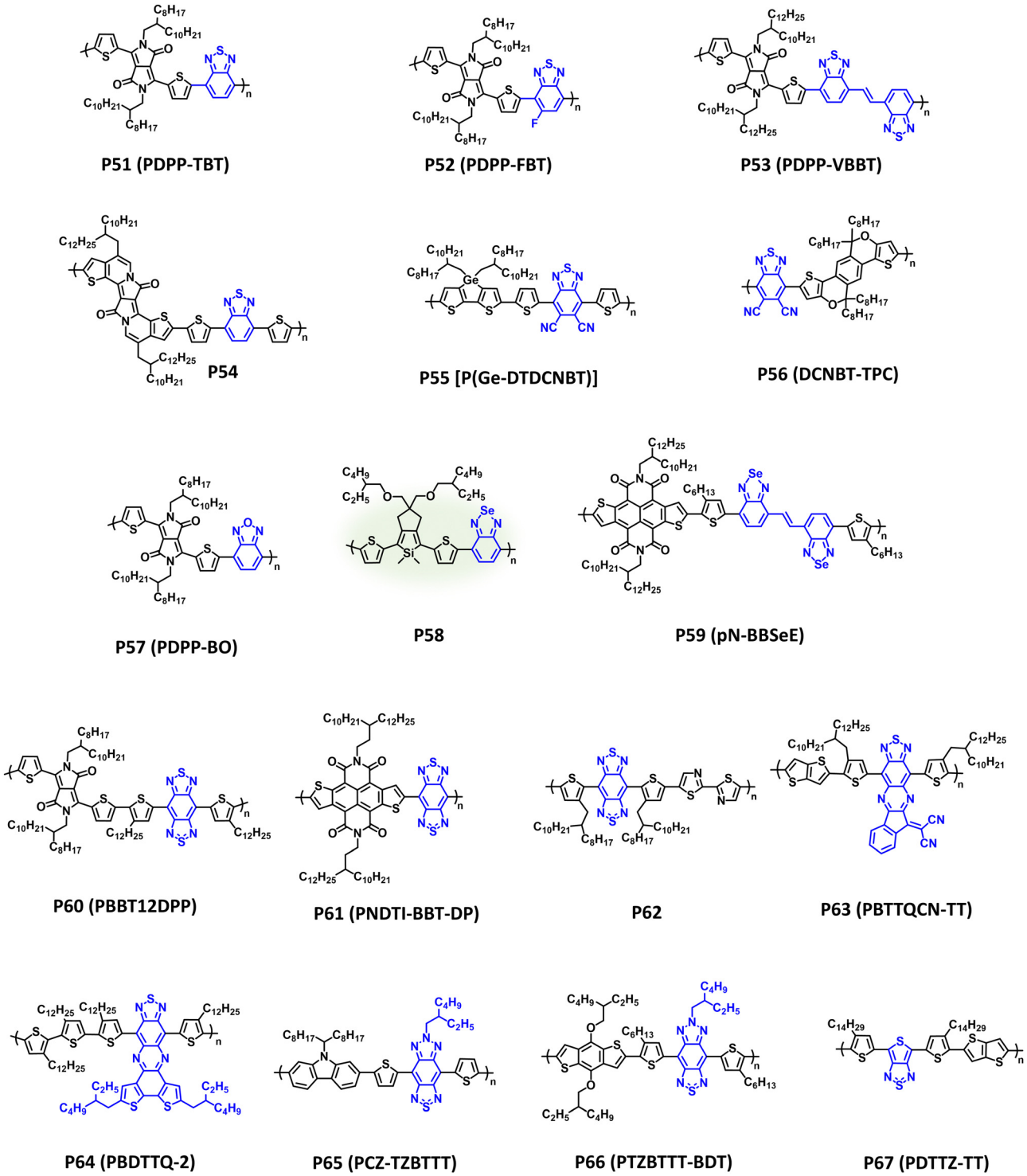

Fig. 11 Select examples of NIR-CPs containing BT analogues. BT NIR-CPs with relatively sustainable syntheses are highlighted in green.

capabilities for harvesting NIR wavelengths allowing it to achieve a remarkable PCE of 10.2% in ternary APSCs.[243]

Chalcogen substitution of benzothiadiazole can also be performed yielding benzooxadiazole or benzoselenodiazole, which is shown with polymers **P57–P59**.[29,245] As described above, chalcogen substitution is an effective way to modifying the energetics and non-covalent interactions of the polymer. Notably, **P57** which substitutes the sulphur in BT for the more electronegative oxygen, provides a significant redshift in optical absorption and narrower bandgap compared to **P51** (λ_{max} = 964 nm and E_g = 1.17 eV).[244] This strategic heteroatom modification enables ambipolar OPTs with D^* = 1 × 10^{12} and 7 × 10^{11} Jones for n-type and p-type operation, respectively, at a NIR wavelength (940 nm). **P58** was synthesized *via* DArP and

Table 4 Tabulated λ_{max}, E_g, ionization potential (IP)/electron affinity (EA), and device performance metrics for BT NIR-CPs and analogues

Polymer[a]	λ_{max} (nm); E_g[b] (eV)	IP/EA (eV)	Device application[c]	Notable performance metric	Ref.
P51 (PDPP-TBT)	915; 1.2	−5.2/−4.0	OFET (BGTC)	μ_h/μ_e = 0.35/0.40 cm^2 V^{-1} s^{-1}	239
P52(PDPP-FBT)	816; 1.20	−5.22/−3.49	OFET (BGTC)	μ_h/μ_e = 0.21/0.42 cm^2 V^{-1} s^{-1}	240
P53 (PDPP-VBBT)	664; 1.35	−5.34/−3.43	OFET (BGTC)	μ_h/μ_e = 0.20/0.15 cm^2 V^{-1} s^{-1}	241
P54	829; 1.27	−5.19/−3.42	OPT (BGBC)	R (850 nm) = 118 A W^{-1}	242
P55 [P(Ge-DTDCNBT)]	754; 1.27	−5.14/−3.77	OFET (TGBC)	μ_e = 2.8 × 10^{-3} cm^2 V^{-1} s^{-1}	58
P56 (DCNBT-TPC)	841; 1.38	−5.51/−3.87	OPV (conventional)	PCE = 10.2%	243
P57 (PDPP-BO)	964; 1.17	−5.4/−4.2	OPT (TGBC)	D^* (940 nm) = 1 × 10^{12} Jones	244
P58	635; 1.58	−5.15/−3.55	OFET (BGTC)	μ_h = 4.65 × 10^{-4} cm^2 V^{-1} s^{-1}	245
P59 (pN-BBSeE)	848; 1.36	−5.53/−4.05	OFET (TGBC)	μ_h/μ_e = 10.65/10.72 cm^2 V^{-1} s^{-1}	29
P60 (PBBT12DPP)	1280; 0.65	−4.55/−3.9	OFET (BGBC)	μ_h/μ_e = 1.17/1.32 cm^2 V^{-1} s^{-1}1	246
P61 (PNDTI-BBT-DP)	914; 0.96	−5.5/−4.4	OFET (BGTC)	μ_h/μ_e = 0.31 cm^2 V^{-1} s^{-1}	247
P62	1106; 1.37	−5.31/−3.94	OFET (BGBC)	μ_h = 0.11 cm^2 V^{-1} s^{-1}	248
P63 (PBTTQCN-TT)	1270; 0.66	−5.20/−4.10	OFET (TGBC)	μ_h/μ_e = 1.3 × 10^{-3}/2.0 × 10^{-3} cm^2 V^{-1} s^{-1}	249
P64 (PBDTTQ-2)	978; 1.03	−5.48/−4.01	OFET (BGBC)	μ_h/μ_e = 1.2 × 10^{-3}/6.0 × 10^{-4} cm^2 V^{-1} s^{-1}	250
P65 (PCZ-TZBTTT)	785; 1.35	−5.18/−3.83	OPV (conventional)	PCE = 3.17%	251
P66 (PTZBTTT-BDT)	810; 1.1	−5.14/−4.04	OPD	D^* (800 nm) = 1.75 × 10^{13} Jones	252
P67 (PDTTZ-TT)	865; 0.98	−4.96/−3.98	OPD	D^* (1160 nm) = 7.3 × 10^{12} Jones	10

[a] Abbreviation in parentheses indicates common name. [b] Estimated in all cases using λ_{onset} where optical E_g = 1240/λ_{onset}. [c] Device architecture is indicated in parentheses (see Section 3). n.r. = not reported.

provides broad optical absorption throughout the visible wavelength region and into the NIR.[245] When incorporated into an OFET, **P58** affords a modest hole mobility (μ_h = 4.65 × 10^{-4} cm^2 V^{-1} s^{-1}). **P59 (pN-BBSeE)** incorporates chalcogen substitution and π-extension, as well as NDTI as an additional acceptor unit. This judiciously designed polymer provides strong NIR optical absorption (λ_{max} = 841 nm and E_g = 1.38 eV) with an additional π–π* absorption band present at 515 nm. Additionally, it affords exceptionally high and well balanced ambipolar charge mobilities (μ_h/μ_e = 10.65/10.72 cm^2 V^{-1} s^{-1}).[29]

A further reduction in bandgap and increase in the EA can be accomplished through the addition of a second thiadiazole functionality on BT to yield benzobisthiadiazole (BBT), which is shown with polymers **P60–P62**. Compared to BT polymers **P51–P59**, **P60 (PBBT12DPP)**, which is a dual-acceptor alternating copolymer containing DPP and BBT repeat units, displays a significant red shift in optical absorption (λ_{max} = 1280 nm) with an ultra-narrow optical bandgap of 0.65 eV. **P60 (PBBT12DPP)** was also found to provide desirable ambipolar charge transport in OFETs (μ_h/μ_e = 1.17/1.32 cm^2 V^{-1} s^{-1}) facilitated by the narrow bandgap of the NIR-CP.[246] **P61 (PNDTI-BBT-DP)** also possesses a dual-acceptor alternating copolymer structure incorporating NDTI and BBT. This polymer also affords a very narrow optical band gap of 0.96 eV, and excellent electron mobility (μ_e = 0.31 cm^2 V^{-1} s^{-1}).[247] Lastly, **P62** incorporates bithiazole and BBT providing optical absorption across the visible wavelength range and into the NIR (λ_{max} = 1106 nm and E_g = 1.37 eV). Instead of ambipolar charge transport, only unipolar hole transport (μ_h = 0.11 cm^2 V^{-1} s^{-1}) was observed with **P62**.[248] Employing computational tools to characterize the electronic structure, this was ascribed to a highly localized LUMO on BBT, which was posited as being unfavourable for electron transport. Additional functionalization strategies to alter the optical and electronic properties of BT based polymers are shown with **P63–P67**. **P63 (PBTTQCN-TT)** and **P64 (PBDTTQ-2)** each contain a BT unit with π-extended fused ring system.[249,250] For **P63 (PBTTQCN-TT)** the indanone functionalized thiadazolo[3,4-*g*]quinoxaline unite imparts an ultra-narrow bandgap of 0.66 eV with strong NIR optical absorption (λ_{max} = 1270 nm), and with **P64 (PBDTTQ-2)** an optical bandgap of 1.03 eV is achieved with λ_{max} = 978 nm. **P63 (PBTTQCN-TT)** and **P64 (PBDTTQ-2)** afford ambipolar charge transport, albeit with relatively low charge mobilities (μ_h/μ_e = 1.3 × 10^{-3}/2.0 × 10^{-3} cm^2 V^{-1} s^{-1} and 1.2 × 10^{-3}/6.0 × 10^{-4} cm^2 V^{-1} s^{-1}, respectively). However, **P63 (PBTTQCN-TT)** has also been incorporated into organic phototransistors providing detection up to 1550 nm.[255]

Introduction of a triazole unit to yield [1,2,5]thiadiazolo[3,4-*f*]benzotriazole is an efficient strategy for facilitating electron transport *via* improved EA with an additional handle for tuning the morphology/microstructure *via* sidechain engineering on the triazole unit with polymers **P65 (PCZ-TZBTTT)** and **P66 (PTZBTTT-BDT)** as examples.[251,252] λ_{max}/E_g for **P65 (PCZ-TZBTTT)** and **P66 (PTZBTTT-BDT)** were measured to be 785 nm/1.35 eV and 810 nm/1.1 eV, respectively. Notably, **P65 (PCZ-TZBTTT)** was blended with $PC_{61}BM$ in OPV devices affording a PCE of 3.17%, and **P66 (PTZBTTT-BDT)** was incorporated into OPDs with $PC_{61}BM$ as the acceptor providing a specific detectivity (D^*) of 1.75 × 10^{13} Jones at 800 nm. Lastly, the polymer **P67 (PDTTZ-TT)** incorporates thieno[3,4-*c*]thiadiazole as an acceptor with a simplified structure in place of BT affording a measured λ_{max}/E_g of 865 nm/0.98 eV.[10] When blended with $PC_{71}BM$ in OPDs a detectivity of 7.3 × 10^{12} Jones is achieved at 1160 nm. This is particularly unique D–A polymer structure, since **P67 (PDTTZ-TT)** is composed entirely of functionalized thiophenes with the thieno[3,4-*c*]thiadiazole acceptor unit synthesized within only a few steps, and the polymer shows optical absorption extending from 400–1200 nm.[10]

Overall, BT provides a relative simple structure with a high degree of structural tunability including heteroatom substitution, π-extension, and ring fusion. It has also been polymerized using Suzuki–Miyaura and DArP, which demonstrates improved sustainability for this class of NIR-CPs. In many cases, NIR-CPs incorporating BT provide highly crystalline morphologies with a

polymer orientation that is preferentially edge-on, which is suitable for OFETs. However, as detailed here, there are examples of BT containing NIR-CPs with utility in OPV/OPDs indicating the morphology can be tailored for the desired device application.

4.5 Fused ring electron acceptors (FREAs) and polymerized small-molecule acceptors (PSMAs)

Fused ring electron acceptors (FREAs) have reignited the field of organic small-molecule and polymer solar cells, due to their strong NIR optical absorption that is complimentary to many state-of-the-art donor polymers, excellent electron transport, and morphological stability relative to fullerenes.[5,6,8,256–260] Their characteristic structural features include an expansive π-conjugated network partitioned into different sections of electron donor (D) or acceptor (A) character to yield A–D–A or A–D–A–D–A structures, which have been the topic of many reviews.[5,6,8,256,257] FREAs are typically comprised of an IDT or thieno[2′,3′:4,5]pyrrolo[3,2-*e*:2′,3′-*g*][2,1,3]benzothiadiazole

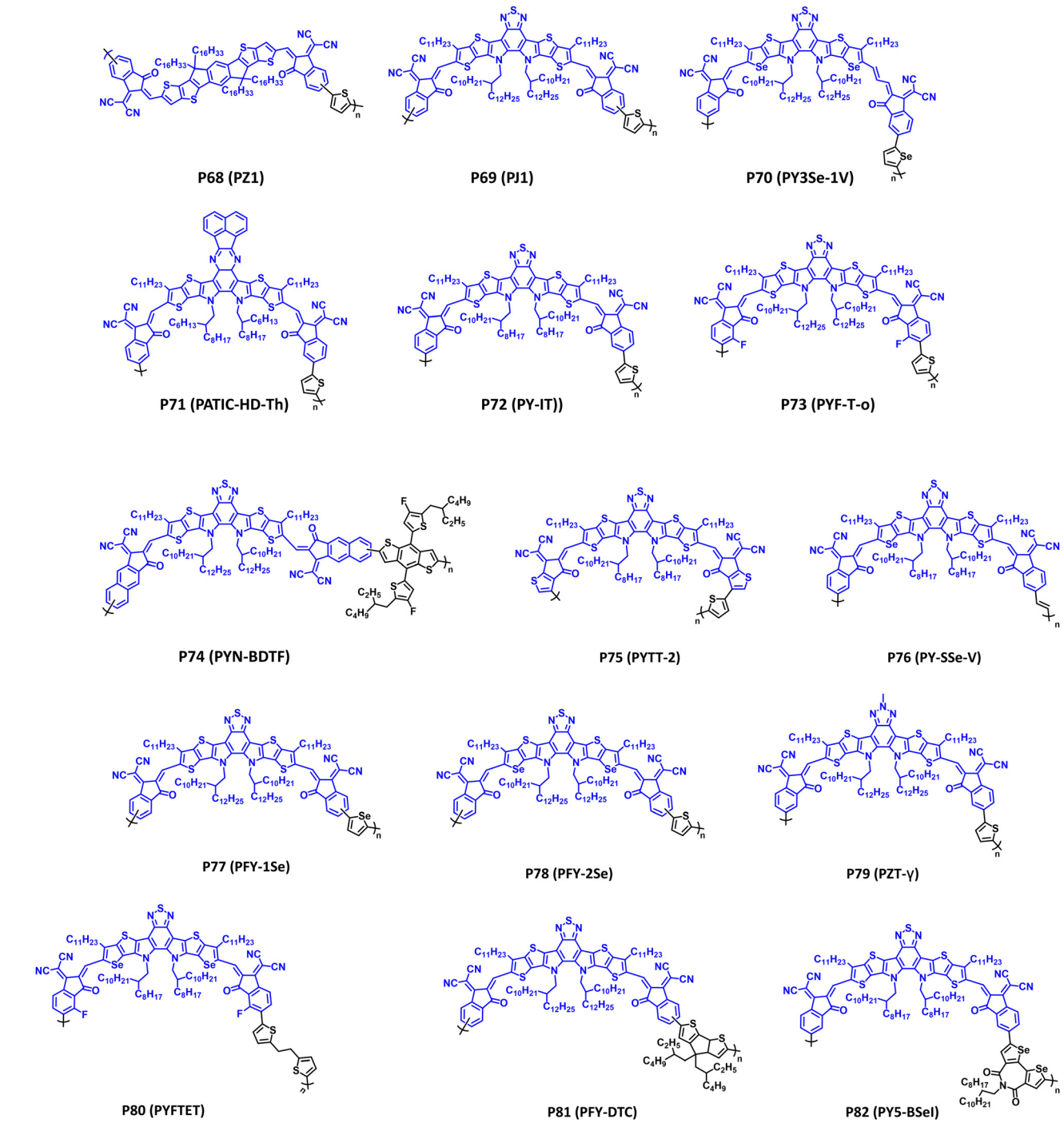

Fig. 12 Select examples of NIR-CPs containing FREAs.

(TPB) core flanked by functionalized indanones, and following polymerization yield a class of polymers referred to as polymerized small-molecule acceptors (PSMAs) with examples provided in Fig. 12 (**P68–P82**) and the optical absorption (λ_{max}), optical bandgap (E_g), IP/EA, and device performance metrics tabulated in Table 5.

Polymers **P68–P71** in Fig. 12 provide a general overview of structural modifications to the central IDT or TPB core observed with FREAs/PSMAs.[261–264] Remarkable levels of structural engineering are observed with these polymers, including sidechain engineering, π-extension, ring fusion, heteroatom substitution, and controlling the polymer regioregularity. Possessing an IDT core, **P68 (PZ1)** was the first demonstration of a PSMA and their utility in APSCs providing complimentary optical absorption (λ_{max} = 704 nm and E_g = 1.55 eV) to the donor polymer **PM6** (Fig. 5).[261] Notably, APSCs with an active layer **P68 (PZ1):PM6** provided a PCE of 11.2%, with exceptional morphological stability (90% retention of the initial PCE after 80 d of storage), and scalability to larger-area devices (1.1 cm^2). **P69 (PJ1)** substitutes the IDT core for TPB providing a significant red shift in the optical absorption (λ_{max} = 798 nm) and reduction in the optical bandgap (E_g = 1.41 eV) relative to **P68 (PZ1)**. When blended with the donor polymer **PBDB-T** a PCE of 14.4% was achieved, and excellent thermal stability of the active layer was observed following annealing at 150 °C for 180 m (PCE = 12.5%).[262] Additionally, with thick (305 nm) active layers a PCE of 12.1% is obtained, indicating potential viability with large scale, foundry-compatible device fabrication. **P70 (PY3Se-1V)** provides an example of π-extension *via* a vinylene spacer and heteroatom substitution *via* selenophene, which is described further with polymers **P76–P79**.[263] The incorporation of the vinylene spacer was found to extend the optical absorption of **P70 (PY3Se-1V)** deeper into the NIR wavelength region providing a λ_{max}/E_g of 850 nm/1.25 eV.[263] **P70 (PY3Se-1V)** was blended with **PBDB-T** in APSCs (PCE = 13.2%) and **P3HT** in OPDs [R (960 nm) = 28 A W^{-1}]. Lastly, **P71 (PATIC-HD-Th)** provides an example of modification of the TPB central core *via* incorporation of quinoxaline analogue derived from phenanthraquinone.[264] A blue shift in optical absorption (λ_{max} = 803 nm) relative to **P68–P70** was observed, and **P71 (PATIC-HD-Th)** provided a PCE of 12.47% in APSCs when blended with **PBDB-T**.

Structural modification of the indanone linker in PSMAs can also be accomplished, which is highlighted with polymers **P72–P75**. This includes synthesis of single structural isomers to control regioregularity [**P72 (PY-IT)**], heteroatom modification [**P73 (PYF-T-o)**], π-extension [**P74 (PYN-BDTF)**], and modification of indanone to incorporate other aromatic heterocycles [**P75 (PYTT-2)**].[21,265–267,274] Controlling the regioregularity of the CP structure from the regio-random **P69 (PJ1)** to the regio-regular **P72 (PY-IT)** yields a red shift in the optical absorption (λ_{max} = 808 nm) and boosts the APSC PCE to 15.05% when blended with **PM6**.[265] Additionally, diligent optimization of the active layer morphology *via* the introduction of solid additives into **PM6:P72 (PY-IT)** blends affords a landmark APSC PCE of 18.3%.[274] Incorporating both strategies of controlling regio-selectivity and heteroatom incorporation, **P73 (PYF-T-o)** employs a fluorination strategy to modify the optical properties and polymer self-assembly.[266] **P73 (PYF-T-o)** provides a red shift in optical absorption (λ_{max} = 824 nm) relative to **P72 (PY-IT)** indicating increased π-orbital overlap and intermolecular interactions, and **PM6:P73 (PYF-T-o)** blends provide a boost in APSC PCE to 15.2%. **P74 (PYN-BDTF)** introduces a π-extended indanone group providing a redshift in the optical absorption (λ_{max} = 820 nm) relative to **P72 (PY-IT)**.[21] Incorporation of the fluorinated donor comonomer with **P74 (PYN-BDTF)** in blends with **PM6** provided a preferential face on orientation and improved crystallinity relative to the non-fluorinated analogue affording a PCE of 13.22%. **P75 (PYTT-2)** incorporates a thiophene analogue of indanone, which provides a regioregular configuration compared to the regio-random configuration with **P69 (PJ1)**. The thiophene functionalized end-group provides desirable optical properties (λ_{max} = 832 nm and E_g = 1.49 eV) and a PCE of 14.32% when blended with **PBDB-T**. Additionally, it provides a robust morphology with 80% PCE retention after annealing at 120 °C for 100 h.

Table 5 Tabulated λ_{max}, E_g, ionization potential (IP)/electron affinity (EA), and device performance metrics for BT NIR-CPs

Polymer[a]	λ_{max} (nm); E_g[b] (eV)	IP/EA (eV)	Device application[c]	Notable performance metric	Ref.
P68 (PZ1)	704; 1.55	−5.74/−3.86	OPV (conventional)	PCE = 11.2%	261
P69 (PJ1)	798; 1.41	−5.64/−3.82	OPV (conventional)	PCE = 14.4%	262
P70 (PY3Se-1V)	850; 1.25	−5.51/−3.90	OPD	R (960 nm) = 28 A W^{-1}	263
P71 (PATIC-HD-Th)	803; n.r.	−5.31/−3.58	OPV (conventional)	PCE = 12.47%	264
P72 (PY-IT)	808; 1.39	−5.68/−3.94	OPV (conventional)	PCE = 15.05%	265
P73 (PYF-T-o)	824; 1.38	−5.73/−3.81	OPV (conventional)	PCE = 15.2%	266
P74 (PYN-BDTF)	820; 1.38	−5.67/−3.77	OPV (conventional)	PCE = 13.22%	21
P75 (PYTT-2)	832; 1.49	−5.73/−3.83	OPV (conventional)	PCE = 14.32%	267
P76 (PY-SSe-V)	912; 1.36	−5.65/−3.78	OPV (conventional)	PCE = 18.14%	268
P77 (PFY-1Se)	800; 1.79	−5.68/−3.89	OPV (conventional)	PCE = 13.8%	269
P78 (PFY-2Se)	825; 1.73	−5.64/−3.91	OPV (conventional)	PCE = 14.7%	269
P79 (PZT-γ)	838; 1.36	−5.57/−3.78	OPV (conventional)	PCE = 15.8%	270
P80 (PYFTET)	866; 1.43	−5.76/−4.08	OPV (conventional)	PCE = 9.53%	271
P81 (PFY-DTC)	n.r.; 1.40	−5.53/−3.87	OPV (conventional)	PCE = 11.08%	272
P82 (PY5-BSeI)	812; 1.35	−5.76/−4.00	OPV (conventional)	PCE = 17.77%	273

[a] Abbreviation in parentheses indicates common name. [b] Estimated in all cases using λ_{onset} where optical $E_g = 1240/\lambda_{onset}$. [c] Device architecture is indicated in parentheses (see Section 3). n.r. = not reported.

As shown with previous NIR-CPs, chalcogen substitution from the commonly employed sulphur/thiophene to its selenium/selenophene analogues or to pnictogens, such as nitrogen, is an effective strategy for tuning the optical properties, polymer energetics, and self-assembly with **P76–P79** provided as examples for FREAs/PSMAs.[268–270] Of particular note is **P76 (PY-SSe-V)**, which possesses a strategic asymmetric substitution of the TPB core to incorporate a single selenophene unit and was polymerized with vinylene to yield a regio-regular NIR-CP suitable for APSCs.[268] **P76 (PY-SSe-V)** afforded a substantial red shift relative to the other PSMAs (λ_{max} = 912 nm) and a PCE of 17.03% when blended with **PM6** in binary devices and 18.14% in ternary solar cells. Jen *et al.* investigated the systematic incorporation of selenium within the **PJ1** framework by preparing polymers **P77 (PFY-1Se)** and **P78 (PFY-2Se)**.[269] Increasing selenium content affords a redshift in optical absorption [λ_{max} = 800 nm/825 nm for **P77 (PFY-1Se)**/**P78 (PFY-2Se)**] and an increase in PCE [PCE = 13.8%/14.7% for **P77 (PFY-1Se)**/**P78 (PFY-2Se)**] with **PBDB-T** as the donor polymer. The improved APSC performance metrics were attributed to increased crystallinity and shorter π–π distances, which are a characteristic of the heavier chalcogens. Next, **P79 (PZT-γ)** is functionalized with a central triazole core rather than BT and incorporates the regio-regular polymerization strategy to achieve broader optical absorption with a λ_{max}/E_g of 838 nm/1.36 eV.[270] It was found the regio-regular structure and incorporation of triazole with **P79 (PZT-γ)** provides ideal phase separation and increased crystalline domains when blended with the donor polymer **PBDB-T**, which affords a PCE of 15.8%.

Lastly, variation of the donor comonomer is another effective strategy for tuning the optical, electronic, morphological/microstructural, and mechanical properties of PSMAs with **P80–P82** as examples.[271–273,275] Notably, **P80 (PYFTET)** incorporates a thienylene-ethylene-thienylene (TET) donor unit, which is the non-conjugated form of TVT.[271,276] This serves as a conjugation break spacer (CBS), which imparts mechanical flexibility and stretchability within the polymer relative to its conjugated counterpart.[277,278] **P80 (PYFTET)** provides a λ_{max}/E_g of 866 nm/1.43 eV with a PCE of 9.53% when blended with **PM6**, and when incorporated into ultra-flexible APSCs using parylene substrates **P80 (PYFTET)** demonstrates 90% PCE retention after 5000 bending cycles at a radius of 14 μm.[271] **P81 (PFY-DTC)** incorporates the strong electron donor unit CDT, which is discussed further in Section 4.6.[272] **P81 (PFY-DTC)** provides extensive coverage of the visible wavelength range into the NIR region with an optical bandgap of 1.40 eV. Blends of **PBDB-T:P81 (PFY-DTC)** displayed strong aggregation and large crystalline domain sizes *via* GIWAXS and provided PCEs of 11.08% in APSCs. Finally, **P82 (PY5-BSeI)** is unique within this class of polymers since it possesses a dual-acceptor alternating copolymer structure with the strategically designed biselenophene imide comonomer.[273] **P82 (PY5-BSeI)** provides strong optical absorption extending from 400–900 nm with a λ_{max}/E_g of 812 nm/1.35 eV. APSCs incorporating **PM6: P82 (PY5-BSeI)** afforded an exceptional PCE of 17.77%, which was attributed to optimal donor–acceptor phase separation, ideal polymer packing and self-assembly, and high crystallinity.

To summarize, FREAs are a class of repeat units that demonstrate the highest levels of structural engineering in NIR-CPs. They afford state-of-the-art performance metrics in OPV devices and desirable performance in OPDs surpassing fullerene and other acceptor polymers in their ability to harvest solar illumination and generate photocurrent. With that taken into account it is worth noting that the syntheses often invoke arduous synthetic pathways, which can increase costs and tarnish the sustainable aspects OPV seeks to provide.[279] Additionally, PSMAs are typically synthesized *via* Stille polymerization so there are many opportunities for future work to address these deficiencies and develop more sustainable synthetic pathways and polymerization procedures suitable for high-performance PSMAs.

4.6 Cyclopentadithiophene (CDT) and analogues

Although differences in the structure and functionalization of acceptor units have been a primary focus of this review, it is important to highlight the CDT donor unit and its analogues, which have afforded numerous NIR-CPs, due to the strong electron donating capabilities imparted by the fused bithiophene framework, with select examples (**P83–P90**) provided in Fig. 13 and the optical absorption (λ_{max}), optical bandgap (E_g), IP/EA, and device performance metrics tabulated in Table 6. **P83–P86** all possess the CDT donor and various functionalized BT acceptor units with λ_{max}/E_g ranging from 702–920 nm/1.20–1.54 eV.[280–288]

P83 and **P84** incorporate a mono-fluorinated and difluorinated BT acceptor unit copolymerized with CDT.[280,281] **P83** provides a redshift in optical absorption relative to **P84** (λ_{max} = 776 nm *versus* 702 nm, respectively), and **P83** demonstrated excellent ambient stability when incorporated into OFETs with an increase in the initial mobility (μ_h = 0.56 $cm^2\ V^{-1}\ s^{-1}$) by 4.8% after ambient storage for 12 d. **P84** was incorporated into OECTs using the ionic-liquid [EMIM][TFSI] as the electrolyte providing a normalized transconductance ($g_{m,norm}$) of 35.8 S cm^{-1}. Use of an ionic liquid is likely critical here, given the absence of hydrophilic EG_n sidechains to facilitate aqueous electrolyte penetration and uptake.

P85 and **P86 (PCPPC)** each incorporate pyridal[2,1,3]-thiadiazole acceptor units. **P85** was strategically synthesized to ensure a regio-regular structure rather than a random orientation of the pyridal[2,1,3]thiadiazole acceptor. This careful control affords strong NIR optical absorption (λ_{max} = 920 nm and E_g = 1.37 eV) and good hole mobilities (μ_h = 0.4 $cm^2\ V^{-1}\ s^{-1}$). **P86 (PCPPC)** possesses a narrower bandgap (E_g = 1.20 eV) and an elevated conduction band relative to **P85** (−3.41 *versus* −3.70 eV, respectively). Yet, **P86** demonstrated ambipolar charge transport in OFETs (μ_h/μ_e = 1.50/0.41 $cm^2\ V^{-1}\ s^{-1}$), and inverters containing **P86 (PCPPC)** were found to provide a gain of 165.[283]

P87 and **P88**, which possess a bridgehead imine-substituted CDT and an exocyclic olefin substituted CDT as the donor units, respectively, provide broad optical absorption extending far into the NIR (λ_{max}/E_g = 1270 nm/$<$0.5 eV (**P87**) and 1080 nm/0.85 eV (**P88**)). This class of donor unit and the corresponding NIR-CPs were pioneered by Azoulay *et al.* and have demonstrated utility in

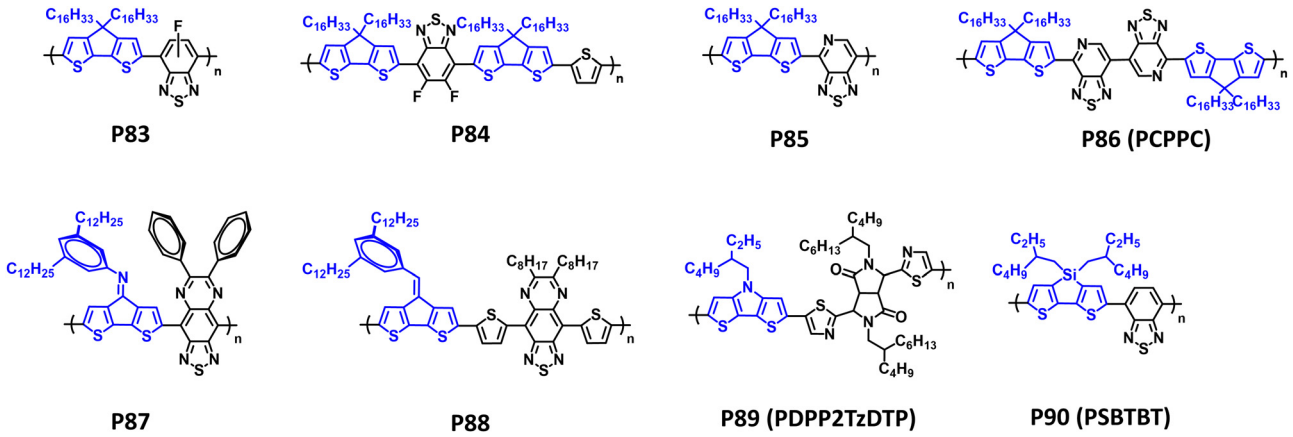

Fig. 13 Select examples of NIR-CPs containing CDT repeat units and analogues.

OPDs with a D^* (1200 nm) of 3×10^{11} Jones provided by **P88** and $PC_{70}BM$ blends.[285,289–291] Lastly, the polymers **P89 (PDPP2TzDTP)** and **P90 (PSBTBT)**, which contain the silole and pyrrole analogues of CDT, each provide narrow bandgaps (E_g = 1.28 and 1.45 eV, respectively).[286,287] **P89 (PDPP2TzDTP)** and **P90 (PSBTBT)** served as a donor polymers in OPV providing PCE*s* of 5.6% and 4.7% when blended with $PC_{70}BM$. More recently, **P90 (PSBTBT)** was incorporated into ternary solar cells with the donor polymer **D18-Cl** and small-molecule acceptor BTP-eC9.[288] In this setting, **P90 (PSBTBT)** provided complementary energy levels to the other components enabling efficient charge transfer and more complimentary spectral coverage across the visible wavelength range and into the NIR. Thus, an excellent PCE of 17.35% was obtained. The application of these structurally simple yet powerful electron donating units into NIR-CPs for ternary solar cells should generate increased research interest for these polymers.

5. Summary and perspective

In summary, an overview of NIR-CPs containing IID, DPP, NDI, BT, FREAs, CDT and analogues with applications in ECDs, OPV, OPDs, OPTs, OFETS, and OECTs was presented. The defining structural characteristics for each polymer class, and strategies for structural engineering to achieve NIR optical absorption and desired performance metrics were also discussed. Common to each of these polymer classes is the alternating D–A copolymer structure, which affords narrow bandgap polymers, tuneable energy levels, and allows for the generation of large libraries of polymers structures.

Of the NIR-CPs presented, it is clear that specific polymer repeat units are best suited for certain organic electronic device applications. Specifically, IID, DPP, NDI, and BT are particularly suited for OFETs and OPTs while FREAs are the optimal choice for achieving state-of-the-art performance metrics in OPVs. Given that all the polymers possess suitable NIR optical absorption, this pairing between polymer and application indicates additional preferred material characteristics, such as energetics and energy level alignment and polymer morphology and microstructure. Thus, even though a polymer may have suitable NIR optical absorption for use in APSCs, the polymer may not have a suitable IP/EA energy offset with the donor polymer to facilitate charge separation. Additionally, the morphology and polymer orientation (*e.g.*, π-face on or edge on) must be carefully considered, since large crystalline domain sizes and polymer aggregation may be detrimental rather than beneficial, and desirable performance metrics are more probable when the orientation of the polymer π–π stacking directions aligns with the direction of charge transport, *e.g.* vertical direction for OPV or horizontal direction for OFET.

Currently, there are limited examples of NIR-CPs in ECDs that can match the performance metrics of CPs with optical switching in the visible wavelength range (ΔT% = 60–80%, t_{95} < 1.0 s, and cycling stability >3000 cycles).[2,292] Thus, there is significant opportunity here for the development of more

Table 6 Tabulated λ_{max}, E_g, ionization potential (IP)/electron affinity (EA), and device performance metrics for CDT NIR-CPs and analogues

Polymer[a]	λ_{max} (nm); E_g[b] (eV)	IP/EA (eV)	Device application[c]	Notable performance metric	Ref.
P83	776; 1.54	−5.05/−3.30	OFET (BGBC)	μ_h = 0.56 $cm^2\ V^{-1}\ s^{-1}$	280
P84	702; 1.46	−5.21/−2.85	OECT (planar)	$g_{m,norm}$ = 35.8 $S\ cm^{-1}$	281
P85	920; 1.37	−5.07/−3.70	OFET (BGTC)	μ_h = 0.4 $cm^2\ V^{-1}\ s^{-1}$	282
P86 (PCPPC)	784; 1.20	−5.28/−3.41	OFET	μ_h/μ_e = 1.5/0.41 $cm^2\ V^{-1}\ s^{-1}$	283
P87	1270; <0.5	−5.15/−4.44	n.r.	n.r.	284
P88	1080; 0.85	−4.80/−3.66	OPD	D^* (1200 nm) = 3×10^{11} Jones	285
P89 (PDPP2TzDTP)	n.r.; 1.28	−5.61/−3.94	OPV	PCE = 5.6%	286
P90 (PSBTBT)	n.r.; 1.45	−5.05/−3.27	OPV	PCE = 17.35%	288

[a] Abbreviation in parentheses indicates common name. [b] Estimated in all cases using λ_{onset} where optical $E_g = 1240/\lambda_{onset}$. [c] Device architecture is indicated in parentheses (see Section 3). n.r. = not reported.

electrochemically robust NIR-CPs. Additionally, the development of ultra-flexible and stretchable organic NIR-ECDs lags behind OFET and OPV.[41,293] With increasing research interest in wearable electronics, e-skin, soft robotics, and IoT applications, the potential for NIR-ECDs to advance capabilities in thermal energy management, energy storage, and active camouflage is significant.[294]

For OPV, there has been rapid development of APSC performance metrics since the discovery of PSMAs. However, the PCE for APSCs still falls behind donor polymer:acceptor small-molecule blends, which have certified PCEs approaching 20%.[295] As with ECDs, the development of flexible and stretchable OPVs with uncompromised performance metrics remains a continued challenge. It is foreseeable that the continued exploration and incorporation of new functionalities, such as hydrogen bonding groups or moieties capable of cross-linking, will assist in the development of more mechanically robust NIR-CPs.[131,296–298]

Aside from developing more mechanically robust materials, another aspect to consider is the advancement of materials operation in extreme environments. Recently, there have been developments in the fabrication of polymer composite materials for thermally robust OFETs and gas sensors where temperatures were set to 220 °C while maintaining hole mobilities >2.0 cm^2 V^{-1} s^{-1}.[299,300] These CP and non-conjugated polymer composite materials enable operation at extreme temperatures, which opens new opportunities for organic electronics where previously only inorganics offered viable technologies. This research area could be expanded to include NIR-CPs in OPV, where thermal stability test are often <100 °C, and ECDs where device operational stability at temperatures of 180 °C has been demonstrated.[301]

Opportunities to further increase sustainability in polymer synthesis and processing should also not be ignored. Currently, DArP has demonstrated utility for multiple classes of CPs; however, the successful application of this polymerization methodology towards PSMAs to achieve convergence in performance metrics with polymers synthesized *via* Stille polymerization has yet to be disclosed, to our knowledge. Additionally, the FREA repeat units incorporated into PSMAs often invoke arduous synthetic pathways that diminish the overall sustainability of OPV. Thus, the grand challenge of identifying structurally simple acceptor polymers while still maintaining high PCEs ($>15\%$) remains an outstanding challenge. Additionally, the solution processing of NIR-CPs often requires toxic halogenated solvents, and so identifying a suitable replacement that can be broadly applied across the field of organic electronics is imperative.

It is envisioned that the broad scope presentation of NIR-CPs provided here will inspire that next generation of structural developments to achieve improved performance metrics or unlock new technological capabilities. It is important to note that the structural advancements are directly tied to an improved understanding of the device operation and underlying physics, and in many instances the performance metrics obtained from device characterization serve as a feedback loop for tailoring polymer design. Thus, the continuity of organic electronics and the continued advancement of NIR-CP structural development is reliant on furthering interdisciplinary interactions between synthetic chemists, materials scientists, engineers, and physicists.

Conflicts of interest

There are no conflicts to declare.

Acknowledgements

The authors gratefully acknowledge support from the UT System STARS Program and UTEP Startup Awards.

References

1 C. M. Amb, A. L. Dyer and J. R. Reynolds, *Chem. Mater.*, 2011, **23**, 397–415.
2 X. Li, K. Perera, J. He, A. Gumyusenge and J. Mei, *J. Mater. Chem. C*, 2019, **7**, 12761–12789.
3 H. Fu, L. Zhang, Y. Dong, C. Zhang and W. Li, *Mater. Chem. Front.*, 2023, **7**, 2337–2358.
4 C. Gu, A.-B. Jia, Y.-M. Zhang and S. X.-A. Zhang, *Chem. Rev.*, 2022, **122**, 14679–14721.
5 L. Zhang, Z. Yao, H. Wang, J. Zhang, X. Ma and F. Zhang, *Sol. RRL*, 2023, **7**, 2300219.
6 T. Wang, M. Chen, R. Sun and J. Min, *Chem*, 2023, **9**, 1702–1767.
7 Y. Cai, L. Huo and Y. Sun, *Adv. Mater.*, 2017, 1605437.
8 G. Zhang, F. R. Lin, F. Qi, T. Heumüller, A. Distler, H.-J. Egelhaaf, N. Li, P. C. Y. Chow, C. J. Brabec, A. K.-Y. Jen and H.-L. Yip, *Chem. Rev.*, 2022, **122**, 14180–14274.
9 C. Liu, L. Shao, S. Chen, Z. Hu, H. Cai and F. Huang, *Prog. Polym. Sci.*, 2023, **143**, 101711.
10 X. Cao, J. Tong, Z. He, M. Zhang, X. Zhang, J. Ma, P. Gao, J. Li, P. Zhang, C. Wang, Y. Xia and H. Wu, *Dyes Pigm.*, 2018, **158**, 319–325.
11 H. Ren, J.-D. Chen, Y.-Q. Li and J.-X. Tang, *Adv. Sci.*, 2021, **8**, 2002418.
12 Q. Li, Y. Guo and Y. Liu, *Chem. Mater.*, 2019, **31**, 6359–6379.
13 P. Hu, X. He and H. Jiang, *InfoMat*, 2021, **3**, 613–630.
14 S. Griggs, A. Marks, H. Bristow and I. McCulloch, *J. Mater. Chem. C*, 2021, **9**, 8099–8128.
15 T. Leydecker, Z. M. Wang, F. Torricelli and E. Orgiu, *Chem. Soc. Rev.*, 2020, **49**, 7627–7670.
16 S. Park, S. H. Kim, H. H. Choi, B. Kang and K. Cho, *Adv. Funct. Mater.*, 2020, **30**, 1904590.
17 J. Rivnay, S. Inal, A. Salleo, R. M. Owens, M. Berggren and G. G. Malliaras, *Nat. Rev. Mater.*, 2018, **3**, 17086.
18 S. T. M. Tan, A. Gumyusenge, T. J. Quill, G. S. LeCroy, G. E. Bonacchini, I. Denti and A. Salleo, *Adv. Mater.*, 2022, 2110406.

19 M. Moser, J. F. Ponder Jr., A. Wadsworth, A. Giovannitti and I. McCulloch, *Adv. Funct. Mater.*, 2019, **29**, 1807033.
20 Y. Wang, S. Wustoni, J. Surgailis, Y. Zhong, A. Koklu and S. Inal, *Nat. Rev. Mater.*, 2024, **9**, 249–265.
21 N. Su, R. Ma, G. Li, T. Liu, L.-W. Feng, C. Lin, J. Chen, J. Song, Y. Xiao, J. Qu, X. Lu, V. K. Sangwan, M. C. Hersam, H. Yan, A. Facchetti and T. J. Marks, *ACS Energy Lett.*, 2021, **6**, 728–738.
22 D. Meng, R. Zheng, Y. Zhao, E. Zhang, L. Dou and Y. Yang, *Adv. Mater.*, 2022, **34**, 2107330.
23 C. J. M. Emmott, J. A. Röhr, M. Campoy-Quiles, T. Kirchartz, A. Urbina, N. J. Ekins-Daukes and J. Nelson, *Energy Environ. Sci.*, 2015, **8**, 1317–1328.
24 E. Pascual-San-José, G. Sadoughi, L. Lucera, M. Stella, E. Martínez-Ferrero, G. E. Morse, M. Campoy-Quiles and I. Burgués-Ceballos, *J. Mater. Chem. A*, 2020, **8**, 9882–9895.
25 J. Niu, Y. Wang, X. Zou, Y. Tan, C. Jia, X. Weng and L. Deng, *Appl. Mater. Today*, 2021, **24**, 101073.
26 Z. Wu, Q. Zhao, X. Luo, H. Ma, W. Zheng, J. Yu, Z. Zhang, K. Zhang, K. Qu, R. Yang, N. Jian, J. Hou, X. Liu, J. Xu and B. Lu, *Chem. Mater.*, 2022, **34**, 9923–9933.
27 Y. Yuan, G. Giri, A. L. Ayzner, A. P. Zoombelt, S. C. B. Mannsfeld, J. Chen, D. Nordlund, M. F. Toney, J. Huang and Z. Bao, *Nat. Commun.*, 2014, **5**, 3005.
28 B. Park, H. Kang, Y. H. Ha, J. Kim, J.-H. Lee, K. Yu, S. Kwon, S.-Y. Jang, S. Kim, S. Jeong, S. Hong, S. Byun, S.-K. Kwon, Y.-H. Kim and K. Lee, *Adv. Sci.*, 2021, **8**, 2100332.
29 D. Liu, Y. Zhao, J. Zhang, Z. Wei, Y. Liu and Y. Wang, *Angew. Chem., Int. Ed.*, 2024, e202400061.
30 J. Han, X. Rong, C. Xu, Y. Deng, Y. Geng, G. Dong and L. Duan, *Adv. Electron. Mater.*, 2023, **9**, 2201288.
31 F. P. García de Arquer, A. Armin, P. Meredith and E. H. Sargent, *Nat. Rev. Mater.*, 2017, **2**, 16100.
32 C. Xie, X.-T. Lu, X.-W. Tong, Z.-X. Zhang, F.-X. Liang, L. Liang, L.-B. Luo and Y.-C. Wu, *Adv. Funct. Mater.*, 2019, **29**, 1806006.
33 Y. Ma, Y. Zhang and W. W. Yu, *J. Mater. Chem. C*, 2019, **7**, 13662–13679.
34 C. Liu, J. Guo, L. Yu, J. Li, M. Zhang, H. Li, Y. Shi and D. Dai, *Light: Sci. Appl.*, 2021, **10**, 123.
35 N. Hiremath, R. Kumar, K. C. Hwang, I. Banerjee, S. Thangudu and R. Vankayala, *ACS Appl. Nano Mater.*, 2022, **5**, 1719–1733.
36 R. M. Pankow and B. C. Thompson, *Polymer*, 2020, **207**, 122874.
37 P.-L. T. Boudreault, A. Najari and M. Leclerc, *Chem. Mater.*, 2011, **23**, 456–469.
38 B. C. Thompson and J. M. J. Fréchet, *Angew. Chem., Int. Ed.*, 2008, **47**, 58–77.
39 G. Gunbas and L. Toppare, *Chem. Commun.*, 2012, **48**, 1083–1101.
40 J. E. Anthony, A. Facchetti, M. Heeney, S. R. Marder and X. Zhan, *Adv. Mater.*, 2010, **22**, 3876–3892.
41 J. C. Yang, J. Mun, S. Y. Kwon, S. Park, Z. Bao and S. Park, *Adv. Mater.*, 2019, **31**, 1904765.
42 E. E. Havinga, W. ten Hoeve and H. Wynberg, *Polym. Bull.*, 1992, **29**, 119–126.
43 E. E. Havinga, W. ten Hoeve and H. Wynberg, *Synth. Met.*, 1993, **55**, 299–306.
44 J. Kuwabara, Y. Fujie, K. Maruyama, T. Yasuda and T. Kanbara, *Macromolecules*, 2016, **49**, 9388–9395.
45 M. Streiter, D. Beer, F. Meier, C. Göhler, C. Lienert, F. Lombeck, M. Sommer and C. Deibel, *Adv. Funct. Mater.*, 2019, **29**, 1903936.
46 J. B. Howard and B. C. Thompson, *Macromol. Chem. Phys.*, 2017, **218**, 1700255.
47 Z. Bao, W. K. Chan and L. Yu, *J. Am. Chem. Soc.*, 1995, **117**, 12426–12435.
48 Z. Bao, W. Chan and L. Yu, *Chem. Mater.*, 1993, **5**, 2–3.
49 L. Sun, X. Xu, S. Song, Y. Zhang, C. Miao, X. Liu, G. Xing and S. Zhang, *Macromol. Rapid Commun.*, 2019, **40**, 1900074.
50 G. Li, X. Zhang, L. O. Jones, J. M. Alzola, S. Mukherjee, L. Feng, W. Zhu, C. L. Stern, W. Huang, J. Yu, V. K. Sangwan, D. M. DeLongchamp, K. L. Kohlstedt, M. R. Wasielewski, M. C. Hersam, G. C. Schatz, A. Facchetti and T. J. Marks, *J. Am. Chem. Soc.*, 2021, **143**, 6123–6139.
51 B. Shahid, D. Zhu, Q. Wang, X. Yuan, I. Ismail, Y. Wu, Z. Du and R. Yang, *Polym. Int.*, 2020, **69**, 564–570.
52 M. Li, C. An, W. Pisula and K. Müllen, *Acc. Chem. Res.*, 2018, **51**, 1196–1205.
53 M. Planells, B. C. Schroeder and I. McCulloch, *Macromolecules*, 2014, **47**, 5889–5894.
54 M. L. Tang and Z. Bao, *Chem. Mater.*, 2011, **23**, 446–455.
55 Y.-S. Lee, J. Y. Lee, S.-M. Bang, B. Lim, J. Lee and S.-I. Na, *J. Mater. Chem. A*, 2016, **4**, 11439–11445.
56 H. Yu, Z. Qi, J. Yu, Y. Xiao, R. Sun, Z. Luo, A. M. H. Cheung, J. Zhang, H. Sun, W. Zhou, S. Chen, X. Guo, X. Lu, F. Gao, J. Min and H. Yan, *Adv. Energy Mater.*, 2020, **11**, 2003171.
57 W. Zhong, J. Xiao, S. Sun, X.-F. Jiang, L. Lan, L. Ying, W. Yang, H.-L. Yip, F. Huang and Y. Cao, *J. Mater. Chem. C*, 2016, **4**, 4719–4727.
58 A. Casey, Y. Han, Z. Fei, A. J. P. White, T. D. Anthopoulos and M. Heeney, *J. Mater. Chem. C*, 2015, **3**, 265–275.
59 G. L. Gibson, T. M. McCormick and D. S. Seferos, *J. Am. Chem. Soc.*, 2012, **134**, 539–547.
60 R. S. Ashraf, I. Meager, M. Nikolka, M. Kirkus, M. Planells, B. C. Schroeder, S. Holliday, M. Hurhangee, C. B. Nielsen, H. Sirringhaus and I. McCulloch, *J. Am. Chem. Soc.*, 2015, **137**, 1314–1321.
61 S. Shi, H. Wang, P. Chen, M. A. Uddin, Y. Wang, Y. Tang, H. Guo, X. Cheng, S. Zhang, H. Y. Woo and X. Guo, *Polym. Chem.*, 2018, **9**, 3873–3884.
62 A. Patra and M. Bendikov, *J. Mater. Chem.*, 2010, **20**, 422–433.
63 E. I. Carrera and D. S. Seferos, *Macromolecules*, 2014, **48**, 297–308.
64 A. V. Marsh and M. Heeney, *Polym. J.*, 2023, **55**, 375–385.
65 J.-L. Bredas, D. Beljonne, V. Coropceanu and J. Cornil, *Chem. Rev.*, 2004, **104**, 4971–5003.
66 H. Mori, S. Nishinaga, R. Takahashi and Y. Nishihara, *Macromolecules*, 2018, **51**, 5473–5484.
67 H. Mori, R. Hosogi, Y. Minagawa, H. Yamane and Y. Nishihara, *ACS Appl. Polym. Mater.*, 2024, **6**, 3883–3893.

68 G. Bianchi, C. Carbonera, L. Ciammaruchi, N. Camaioni, N. Negarville, F. Tinti, G. Forti, A. Nitti, D. Pasini, A. Facchetti, R. M. Pankow, T. J. Marks and R. Po, *Sol. RRL*, 2022, **6**, 2200643.
69 H. Yao, L. Ye, H. Zhang, S. Li, S. Zhang and J. Hou, *Chem. Rev.*, 2016, **116**, 7397–7457.
70 J. Yuan, Y. Zhang, L. Zhou, G. Zhang, H.-L. Yip, T.-K. Lau, X. Lu, C. Zhu, H. Peng, P. A. Johnson, M. Leclerc, Y. Cao, J. Ulanski, Y. Li and Y. Zou, *Joule*, 2019, **3**, 1140–1151.
71 Y.-J. Cheng, Y.-J. Ho, C.-H. Chen, W.-S. Kao, C.-E. Wu, S.-L. Hsu and C.-S. Hsu, *Macromolecules*, 2012, **45**, 2690–2698.
72 J. Mei and Z. Bao, *Chem. Mater.*, 2014, **26**, 604–615.
73 I. McCulloch, M. Heeney, M. L. Chabinyc, D. DeLongchamp, R. J. Kline, M. Cölle, W. Duffy, D. Fischer, D. Gundlach, B. Hamadani, R. Hamilton, L. Richter, A. Salleo, M. Shkunov, D. Sparrowe, S. Tierney and W. Zhang, *Adv. Mater.*, 2009, **21**, 1091–1109.
74 Y. Liu, J. Zhao, Z. Li, C. Mu, W. Ma, H. Hu, K. Jiang, H. Lin, H. Ade and H. Yan, *Nat. Commun.*, 2014, **5**, 5293.
75 J. Zhao, Y. Li, G. Yang, K. Jiang, H. Lin, H. Ade, W. Ma and H. Yan, *Nat. Energy*, 2016, **1**, 15027.
76 J. Rivnay, S. C. B. Mannsfeld, C. E. Miller, A. Salleo and M. F. Toney, *Chem. Rev.*, 2012, **112**, 5488–5519.
77 Y. Wu, S. Schneider, C. Walter, A. H. Chowdhury, B. Bahrami, H.-C. Wu, Q. Qiao, M. F. Toney and Z. Bao, *J. Am. Chem. Soc.*, 2020, **142**, 392–406.
78 A. Giovannitti, D.-T. Sbircea, S. Inal, C. B. Nielsen, E. Bandiello, D. A. Hanifi, M. Sessolo, G. G. Malliaras, I. McCulloch and J. Rivnay, *Proc. Natl. Acad. Sci. U. S. A.*, 2016, **113**, 12017.
79 Y. Kim, J. Choi, C. Lee, Y. Kim, C. Kim, T. L. Nguyen, B. Gautam, K. Gundogdu, H. Y. Woo and B. J. Kim, *Chem. Mater.*, 2018, **30**, 5663–5672.
80 C. Lee, H. R. Lee, J. Choi, Y. Kim, T. L. Nguyen, W. Lee, B. Gautam, X. Liu, K. Zhang, F. Huang, J. H. Oh, H. Y. Woo and B. J. Kim, *Adv. Energy Mater.*, 2018, **8**, 1802674.
81 I. McCulloch, M. Heeney, C. Bailey, K. Genevicius, I. MacDonald, M. Shkunov, D. Sparrowe, S. Tierney, R. Wagner, W. Zhang, M. L. Chabinyc, R. J. Kline, M. D. McGehee and M. F. Toney, *Nat. Mater.*, 2006, **5**, 328–333.
82 S. Moro, N. Siemons, O. Drury, D. A. Warr, T. A. Moriarty, L. M. A. Perdigão, D. Pearce, M. Moser, R. K. Hallani, J. Parker, I. McCulloch, J. M. Frost, J. Nelson and G. Costantini, *ACS Nano*, 2022, **16**, 21303–21314.
83 C. Liu, C. Xiao, J. Wang, B. Liu, Y. Hao, J. Guo, J. Song, Z. Tang, Y. Sun and W. Li, *Macromolecules*, 2022, **55**, 5964–5974.
84 L. Sun, N. Sun, L. Bai, X. An, B. Liu, C. Sun, L. Fan, C. Wei, Y. Han, M. Yu, J. Lin, D. Lu, N. Wang, L. Xie, K. Shen, X. Zhang, Y. Xu, J. Cabanillas-Gonzalez and W. Huang, *Chin. Chem. Lett.*, 2019, **30**, 1959–1964.
85 C. Pan, Z. Guo and J. Xu, *ACS Appl. Eng. Mater.*, 2024, **2**, 49–55.
86 J. Neu, S. Samson, K. Ding, J. J. Rech, H. Ade and W. You, *Macromolecules*, 2023, **56**, 2092–2103.
87 Z. Chen, L. Yan, J. J. Rech, J. Hu, Q. Zhang and W. You, *ACS Appl. Polym. Mater.*, 2019, **1**, 804–814.
88 Z. Li, L. Ying, P. Zhu, W. Zhong, N. Li, F. Liu, F. Huang and Y. Cao, *Energy Environ. Sci.*, 2019, **12**, 157–163.
89 J. Mei, D. H. Kim, A. L. Ayzner, M. F. Toney and Z. Bao, *J. Am. Chem. Soc.*, 2011, **133**, 20130–20133.
90 M. Moser, L. R. Savagian, A. Savva, M. Matta, J. F. Ponder, T. C. Hidalgo, D. Ohayon, R. Hallani, M. Reisjalali, A. Troisi, A. Wadsworth, J. R. Reynolds, S. Inal and I. McCulloch, *Chem. Mater.*, 2020, **32**, 6618–6628.
91 A. A. Advincula, A. L. Jones, K. J. Thorley, A. M. Österholm, J. F. Ponder and J. R. Reynolds, *Chem. Mater.*, 2022, **34**, 4633–4645.
92 R. M. Pankow, B. Kerwin, Y. Cho, S. Jeong, G. Forti, B. Musolino, C. Yang, A. Facchetti and T. J. Marks, *Adv. Funct. Mater.*, 2023, **34**, 2309428.
93 W. Huang, J. Chen, Y. Yao, D. Zheng, X. Ji, L.-W. Feng, D. Moore, N. R. Glavin, M. Xie, Y. Chen, R. M. Pankow, A. Surendran, Z. Wang, Y. Xia, L. Bai, J. Rivnay, J. Ping, X. Guo, Y. Cheng, T. J. Marks and A. Facchetti, *Nature*, 2023, **613**, 496–502.
94 J. Kim, R. M. Pankow, Y. Cho, I. D. Duplessis, F. Qin, D. Meli, R. Daso, D. Zheng, W. Huang, J. Rivnay, T. J. Marks and A. Facchetti, *Nat. Electron.*, 2024, **7**, 234–243.
95 Z.-F. Yao, J.-Y. Wang and J. Pei, *Prog. Polym. Sci.*, 2023, **136**, 101626.
96 N. A. Kukhta and C. K. Luscombe, *Chem. Commun.*, 2022, **58**, 6982–6997.
97 W. J. Mullin, S. A. Sharber and S. W. Thomas III, *J. Polym. Sci.*, 2021, **59**, 1643–1663.
98 A. Salleo, *Mater. Today*, 2007, **10**, 38–45.
99 R. Noruzi, E. Lim, B. S. S. Pokuri, M. L. Chabinyc and B. Ganapathysubramanian, *npj Comput. Mater.*, 2022, **8**, 38.
100 S. E. Chen, L. Q. Flagg, J. W. Onorato, L. J. Richter, J. Guo, C. K. Luscombe and D. S. Ginger, *J. Mater. Chem. A*, 2022, **10**, 10738–10749.
101 C. G. Bischak, L. Q. Flagg, K. Yan, T. Rehman, D. W. Davies, R. J. Quezada, J. W. Onorato, C. K. Luscombe, Y. Diao, C.-Z. Li and D. S. Ginger, *J. Am. Chem. Soc.*, 2020, **142**, 7434–7442.
102 H. Sirringhaus, M. Bird and N. Zhao, *Adv. Mater.*, 2010, **22**, 3893–3898.
103 G. Horowitz, *Adv. Mater.*, 1998, **10**, 365–377.
104 S. Holliday, Y. Li and C. K. Luscombe, *Prog. Polym. Sci.*, 2017, **70**, 34–51.
105 K. A. Mazzio and C. K. Luscombe, *Chem. Soc. Rev.*, 2015, **44**, 78–90.
106 N. S. Gobalasingham, S. Noh, J. B. Howard and B. C. Thompson, *ACS Appl. Mater. Interfaces*, 2016, **8**, 27931–27941.
107 G. G. Odian, *Principles of polymerization*, Wiley-Interscience, Hoboken, NJ, 4th edn, 2004.
108 A. Mahmood and J.-L. Wang, *Sol. RRL*, 2020, **4**, 2000337.
109 P. Müller-Buschbaum, *Adv. Mater.*, 2014, **26**, 7692–7709.
110 M. Pandey, N. Kumari, S. Nagamatsu and S. S. Pandey, *J. Mater. Chem. C*, 2019, **7**, 13323–13351.
111 G. Cai, J. Wang and P. S. Lee, *Acc. Chem. Res.*, 2016, **49**, 1469–1476.
112 D. K. Pathak and H. C. Moon, *Mater. Horiz.*, 2022, **9**, 2949–2975.

113 A. L.-S. Eh, A. W. M. Tan, X. Cheng, S. Magdassi and P. S. Lee, *Energy Technol.*, 2018, **6**, 33–45.
114 P. M. Beaujuge and J. R. Reynolds, *Chem. Rev.*, 2010, **110**, 268–320.
115 M. Nikolou, A. L. Dyer, T. T. Steckler, E. P. Donoghue, Z. Wu, N. C. Heston, A. G. Rinzler, D. B. Tanner and J. R. Reynolds, *Chem. Mater.*, 2009, **21**, 5539–5547.
116 X. Cheng, Y. Ma, X. Ju, W. Zhao, J. Zhao, Q. Li, Z. Sang, H. Du and Y. Zhang, *Synth. Met.*, 2020, **270**, 116589.
117 Y. Zhang, L. Kong, Y. Zhang, H. Du, J. Zhao, S. Chen, Y. Xie and Y. Wang, *Org. Electron.*, 2020, **81**, 105685.
118 J. A. Kerszulis, R. H. Bulloch, N. B. Teran, R. M. W. Wolfe and J. R. Reynolds, *Macromolecules*, 2016, **49**, 6350–6359.
119 L. A. Estrada, J. J. Deininger, G. D. Kamenov and J. R. Reynolds, *ACS Macro Lett.*, 2013, **2**, 869–873.
120 C. J. Brabec, A. Distler, X. Du, H.-J. Egelhaaf, J. Hauch, T. Heumueller and N. Li, *Adv. Energy Mater.*, 2020, **10**, 2001864.
121 Z. Wang, K. Gao, Y. Kan, M. Zhang, C. Qiu, L. Zhu, Z. Zhao, X. Peng, W. Feng, Z. Qian, X. Gu, A. K.-Y. Jen, B. Z. Tang, Y. Cao, Y. Zhang and F. Liu, *Nat. Commun.*, 2021, **12**, 332.
122 G. Feng, J. Li, F. J. M. Colberts, M. Li, J. Zhang, F. Yang, Y. Jin, F. Zhang, R. A. J. Janssen, C. Li and W. Li, *J. Am. Chem. Soc.*, 2017, **139**, 18647–18656.
123 G. Wang, F. S. Melkonyan, A. Facchetti and T. J. Marks, *Angew. Chem., Int. Ed.*, 2018, **58**, 4129.
124 N. K. Elumalai and A. Uddin, *Energy Environ. Sci.*, 2016, **9**, 391–410.
125 D. Gupta, S. Mukhopadhyay and K. S. Narayan, *Sol. Energy Mater. Sol. Cells*, 2010, **94**, 1309–1313.
126 M.-H. Jao, H.-C. Liao and W.-F. Su, *J. Mater. Chem. A*, 2016, **4**, 5784–5801.
127 R. M. Pankow, J. Wu, A. Harbuzaru, B. Kerwin, Y. Chen, R. P. Ortiz, A. Facchetti and T. J. Marks, *Chem. Mater.*, 2022, **34**, 3267–3279.
128 J. Wu, C. Fu, R. M. Pankow, Y. Chen, D. Zheng, Z. Lu, Y. Huang, T. J. Marks and A. Facchetti, *Chem. Mater.*, 2023, **35**, 10106–10118.
129 T. J. Aldrich, A. S. Dudnik, N. D. Eastham, E. F. Manley, L. X. Chen, R. P. H. Chang, F. S. Melkonyan, A. Facchetti and T. J. Marks, *Macromolecules*, 2018, **51**, 9140–9155.
130 N. S. Gobalasingham, R. M. Pankow, S. Ekiz and B. C. Thompson, *J. Mater. Chem. A*, 2017, **5**, 14101–14113.
131 J. Y. Oh, S. Rondeau-Gagné, Y.-C. Chiu, A. Chortos, F. Lissel, G.-J. N. Wang, B. C. Schroeder, T. Kurosawa, J. Lopez, T. Katsumata, J. Xu, C. Zhu, X. Gu, W.-G. Bae, Y. Kim, L. Jin, J. W. Chung, J. B.-H. Tok and Z. Bao, *Nature*, 2016, **539**, 411–415.
132 G. Dufil, I. Bernacka-Wojcik, A. Armada-Moreira and E. Stavrinidou, *Chem. Rev.*, 2022, **122**, 4847–4883.
133 R. Kubota, Y. Sasaki, T. Minamiki and T. Minami, *ACS Sens.*, 2019, **4**, 2571–2587.
134 Z. A. Lamport, H. F. Haneef, S. Anand, M. Waldrip and O. D. Jurchescu, *J. Appl. Phys.*, 2018, **124**, 071101.
135 Y.-C. Lin, W.-C. Yang, Y.-C. Chiang and W.-C. Chen, *Small Sci.*, 2022, **2**, 2100109.
136 Y. Guo, X. Yang, L. Wang, J. Duan, Y. Zhou, C. B. Nielsen, Y. Yu, J. Yang, Y. Guo, Z. Li, W. Yue, Y. Liu and I. McCulloch, *Macromolecules*, 2021, **54**, 10312–10320.
137 J. F. Ponder Jr, H. Chen, A. M. T. Luci, S. Moro, M. Turano, A. L. Hobson, G. S. Collier, L. M. A. Perdigão, M. Moser, W. Zhang, G. Costantini, J. R. Reynolds and I. McCulloch, *ACS Mater. Lett.*, 2021, **3**, 1503–1512.
138 J. Chen, W. Huang, D. Zheng, Z. Xie, X. Zhuang, D. Zhao, Y. Chen, N. Su, H. Chen, R. M. Pankow, Z. Gao, J. Yu, X. Guo, Y. Cheng, J. Strzalka, X. Yu, T. J. Marks and A. Facchetti, *Nat. Mater.*, 2022, **21**, 564–571.
139 S. Inal, J. Rivnay, A.-O. Suiu, G. G. Malliaras and I. McCulloch, *Acc. Chem. Res.*, 2018, **51**, 1368–1376.
140 S. G. Kim, J. S. Han, H. Kim, S. Y. Kim and H. W. Jang, *Adv. Mater. Technol.*, 2018, **3**, 1800457.
141 Y. van de Burgt, A. Melianas, S. T. Keene, G. Malliaras and A. Salleo, *Nat. Electron.*, 2018, **1**, 386–397.
142 M. Berggren, X. Crispin, S. Fabiano, M. P. Jonsson, D. T. Simon, E. Stavrinidou, K. Tybrandt and I. Zozoulenko, *Adv. Mater.*, 2019, **31**, 1805813.
143 D. Ohayon, V. Druet and S. Inal, *Chem. Soc. Rev.*, 2023, **52**, 1001–1023.
144 A. Erhardt, A. Hochgesang, C. R. McNeill and M. Thelakkat, *Adv. Electron. Mater.*, 2023, **9**, 2300026.
145 X. Luo, H. Shen, K. Perera, D. T. Tran, B. W. Boudouris and J. Mei, *ACS Macro Lett.*, 2021, **10**, 1061–1067.
146 R. Stalder, J. Mei, J. Subbiah, C. Grand, L. A. Estrada, F. So and J. R. Reynolds, *Macromolecules*, 2011, **44**, 6303–6310.
147 R. Stalder, J. Mei, K. R. Graham, L. A. Estrada and J. R. Reynolds, *Chem. Mater.*, 2014, **26**, 664–678.
148 Y. Wang, Y. Yu, H. Liao, Y. Zhou, I. McCulloch and W. Yue, *Acc. Chem. Res.*, 2020, **53**, 2855–2868.
149 F. Grenier, B. R. Aïch, Y.-Y. Lai, M. Guérette, A. B. Holmes, Y. Tao, W. W. H. Wong and M. Leclerc, *Chem. Mater.*, 2015, **27**, 2137–2143.
150 T. Lei, J.-H. Dou and J. Pei, *Adv. Mater.*, 2012, **24**, 6457–6461.
151 M. H. Chua, S. H. G. Toh, P. J. Ong, Z. M. Png, Q. Zhu, S. Xiong and J. Xu, *Polym. Chem.*, 2022, **13**, 967–981.
152 Z. S. Parr, J. Borges-González, R. B. Rashid, K. J. Thorley, D. Meli, B. D. Paulsen, J. Strzalka, J. Rivnay and C. B. Nielsen, *Adv. Mater.*, 2022, **34**, 2107829.
153 L. Xu, Z. Zhao, M. Xiao, J. Yang, J. Xiao, Z. Yi, S. Wang and Y. Liu, *ACS Appl. Mater. Interfaces*, 2017, **9**, 40549–40555.
154 J. Yang, Y. Jiang, Z. Zhao, X. Yang, Z. Zhang, J. Chen, J. Li, W. Shi, S. Wang, Y. Guo and Y. Liu, *Natl. Sci. Rev.*, 2022, **9**, nwab145.
155 R. S. Ashraf, A. J. Kronemeijer, D. I. James, H. Sirringhaus and I. McCulloch, *Chem. Commun.*, 2012, **48**, 3939–3941.
156 G. W. P. Van Pruissen, F. Gholamrezaie, M. M. Wienk and R. A. J. Janssen, *J. Mater. Chem.*, 2012, **22**, 20387–20393.
157 N. Nozaki, A. Uva, H. Matsumoto, H. Tran and M. Ashizawa, *RSC Appl. Polym.*, 2024, **2**, 163–171.
158 J. Huang, Z. Mao, Z. Chen, D. Gao, C. Wei, W. Zhang and G. Yu, *Chem. Mater.*, 2016, **28**, 2209–2218.
159 G. Zhang, Z. Ye, P. Li, J. Guo, Q. Wang, L. Tang, H. Lu and L. Qiu, *Polym. Chem.*, 2015, **6**, 3970–3978.

160 K. Shi, W. Zhang, D. Gao, S. Zhang, Z. Lin, Y. Zou, L. Wang and G. Yu, *Adv. Mater.*, 2018, **30**, 1705286.
161 K. Huang, X. Zhao, Y. Du, S. Kim, X. Wang, H. Lu, K. Cho, G. Zhang and L. Qiu, *J. Mater. Chem. C*, 2019, **7**, 7618–7626.
162 X. Wang, F. Zhao, Z. Xue, Y. Yuan, M. Huang, G. Zhang, Y. Ding and L. Qiu, *Adv. Electron. Mater.*, 2019, **5**, 1900174.
163 B. He, A. B. Pun, D. Zherebetskyy, Y. Liu, F. Liu, L. M. Klivansky, A. M. McGough, B. A. Zhang, K. Lo, T. P. Russell, L. Wang and Y. Liu, *J. Am. Chem. Soc.*, 2014, **136**, 15093–15101.
164 B. He, W. T. Neo, T. L. Chen, L. M. Klivansky, H. Wang, T. Tan, S. J. Teat, J. Xu and Y. Liu, *ACS Sustainable Chem. Eng.*, 2016, **4**, 2797–2805.
165 K. J. Fallon, N. Wijeyasinghe, E. F. Manley, S. D. Dimitrov, S. A. Yousaf, R. S. Ashraf, W. Duffy, A. A. Y. Guilbert, D. M. E. Freeman, M. Al-Hashimi, J. Nelson, J. R. Durrant, L. X. Chen, I. McCulloch, T. J. Marks, T. M. Clarke, T. D. Anthopoulos and H. Bronstein, *Chem. Mater.*, 2016, **28**, 8366–8378.
166 J. Yang, Y. Jiang, Z. Tu, Z. Zhao, J. Chen, Z. Yi, Y. Li, S. Wang, Y. Yi, Y. Guo and Y. Liu, *Adv. Funct. Mater.*, 2019, **29**, 1804839.
167 C.-J. Yang and S. A. Jenekhe, *Macromolecules*, 1995, **28**, 1180–1196.
168 A. Bolduc, S. Barik, M. R. Lenze, K. Meerholz and W. G. Skene, *J. Mater. Chem. A*, 2014, **2**, 15620–15626.
169 S. Barik and W. G. Skene, *Polym. Chem.*, 2011, **2**, 1091–1097.
170 T. Lei, M. Guan, J. Liu, H.-C. Lin, R. Pfattner, L. Shaw, A. F. McGuire, T.-C. Huang, L. Shao, K.-T. Cheng, J. B.-H. Tok and Z. Bao, *Proc. Natl. Acad. Sci. U. S. A.*, 2017, **114**, 5107.
171 Y. Ding, F. Zhao, S. Kim, X. Wang, H. Lu, G. Zhang, K. Cho and L. Qiu, *ACS Appl. Mater. Interfaces*, 2020, **12**, 41832–41841.
172 T. Lei, J.-H. Dou, X.-Y. Cao, J.-Y. Wang and J. Pei, *J. Am. Chem. Soc.*, 2013, **135**, 12168–12171.
173 G. Zhang, P. Li, L. Tang, J. Ma, X. Wang, H. Lu, B. Kang, K. Cho and L. Qiu, *Chem. Commun.*, 2014, **50**, 3180–3183.
174 Z. Yan, B. Sun and Y. Li, *Chem. Commun.*, 2013, **49**, 3790–3792.
175 H. Tang, Y. Liang, C. Liu, Z. Hu, Y. Deng, H. Guo, Z. Yu, A. Song, H. Zhao, D. Zhao, Y. Zhang, X. Guo, J. Pei, Y. Ma, Y. Cao and F. Huang, *Nature*, 2022, **611**, 271–277.
176 K. J. Fallon and H. Bronstein, *Acc. Chem. Res.*, 2021, **54**, 182–193.
177 W. Li, W. S. C. Roelofs, M. Turbiez, M. M. Wienk and R. A. J. Janssen, *Adv. Mater.*, 2014, **26**, 3304–3309.
178 M. M. Wienk, M. Turbiez, J. Gilot and R. A. J. Janssen, *Adv. Mater.*, 2008, **20**, 2556–2560.
179 Y. Patil and R. Misra, *J. Mater. Chem. C*, 2019, **7**, 13020–13031.
180 W. K. Chan, Y. Chen, Z. Peng and L. Yu, *J. Am. Chem. Soc.*, 1993, **115**, 11735–11743.
181 Y. Li, P. Sonar, L. Murphy and W. Hong, *Energy Environ. Sci.*, 2013, **6**, 1684–1710.
182 X. Guo, A. Facchetti and T. J. Marks, *Chem. Rev.*, 2014, **114**, 8943–9021.
183 Q. Wang, S. Böckmann, F. Günther, M. Streiter, M. Zerson, A. D. Scaccabarozzi, W. L. Tan, H. Komber, C. Deibel, R. Magerle, S. Gemming, C. R. McNeill, M. Caironi, M. R. Hansen and M. Sommer, *Chem. Mater.*, 2021, **33**, 2635–2645.
184 C. Zhang, W. L. Tan, Z. Liu, Q. He, Y. Li, J. Ma, A. S. R. Chesman, Y. Han, C. R. McNeill, M. Heeney and Z. Fei, *Macromolecules*, 2022, **55**, 4429–4440.
185 J. Kuwabara, N. Takase, T. Yasuda and T. Kanbara, *J. Polym. Sci., Part A: Polym. Chem.*, 2016, **54**, 2337–2345.
186 S. Broll, F. Nübling, A. Luzio, D. Lentzas, H. Komber, M. Caironi and M. Sommer, *Macromolecules*, 2015, **48**, 7481–7488.
187 X. Liu, Y. Guo, Y. Ma, H. Chen, Z. Mao, H. Wang, G. Yu and Y. Liu, *Adv. Mater.*, 2014, **26**, 3631–3636.
188 H. Chen, Y. Guo, G. Yu, Y. Zhao, J. Zhang, D. Gao, H. Liu and Y. Liu, *Adv. Mater.*, 2012, **24**, 4618–4622.
189 R. Gao, P. Yuan, X. Zhang, S. Sang, X.-C. Hang, H. Nan, C. Liu, C. Zhang, X. Gao, F. Chen, X. Guo and Z.-K. Chen, *ACS Appl. Electron. Mater.*, 2019, **1**, 1233–1242.
190 Y. Zheng, S. Zhang, J. B.-H. Tok and Z. Bao, *J. Am. Chem. Soc.*, 2022, **144**, 4699–4715.
191 R. M. Pankow, A. Harbuzaru, D. Zheng, B. Kerwin, G. Forti, I. D. Duplessis, B. Musolino, R. Ponce Ortiz, A. Facchetti and T. J. Marks, *J. Am. Chem. Soc.*, 2023, **145**, 13411–13419.
192 J. Z. Low, W. T. Neo, Q. Ye, W. J. Ong, I. H. K. Wong, T. T. Lin and J. Xu, *J. Polym. Sci., Part A: Polym. Chem.*, 2015, **53**, 1287–1295.
193 C. J. Mueller, C. R. Singh and M. Thelakkat, *J. Polym. Sci., Part B: Polym. Phys.*, 2016, **54**, 639–648.
194 G. Krauss, F. Meichsner, A. Hochgesang, J. Mohanraj, S. Salehi, P. Schmode and M. Thelakkat, *Adv. Funct. Mater.*, 2021, **31**, 2010048.
195 G. Zhang, Y. Fu, Z. Xie and Q. Zhang, *Sol. Energy Mater. Sol. Cells*, 2011, **95**, 1168–1173.
196 Y. Lei, N. Li, W.-K. E. Chan, B. S. Ong and F. Zhu, *Org. Electron.*, 2017, **48**, 12–18.
197 C. J. Mueller, C. R. Singh, M. Fried, S. Huettner and M. Thelakkat, *Adv. Funct. Mater.*, 2015, **25**, 2725–2736.
198 Q. Liu, Y. Wang, A. Kohara, H. Matsumoto, S. Manzhos, K. Feron, S. E. Bottle, J. Bell, T. Michinobu and P. Sonar, *Adv. Funct. Mater.*, 2020, **30**, 1907452.
199 Q. Liu, W. He, Y. Shi, S. Otep, W. L. Tan, S. Manzhos, C. R. McNeill, X. Guo, P. Sonar, T. Michinobu and A. K. K. Kyaw, *Chem. Mater.*, 2022, **34**, 3140–3151.
200 G. Oklem, X. Song, L. Toppare, D. Baran and G. Gunbas, *J. Mater. Chem. C*, 2018, **6**, 2957–2961.
201 Z. Yuan, B. Fu, S. Thomas, S. Zhang, G. DeLuca, R. Chang, L. Lopez, C. Fares, G. Zhang, J.-L. Bredas and E. Reichmanis, *Chem. Mater.*, 2016, **28**, 6045–6049.
202 Z. Chen, D. Gao, J. Huang, Z. Mao, W. Zhang and G. Yu, *ACS Appl. Mater. Interfaces*, 2016, **8**, 34725–34734.
203 D. Gao, Z. Chen, J. Huang, W. Zhang, C. Wei, Z. Lin, D. Li and G. Yu, *J. Mater. Chem. C*, 2017, **5**, 3568–3578.
204 C. Buckley, S. Thomas, M. McBride, Z. Yuan, G. Zhang, J.-L. Bredas and E. Reichmanis, *Chem. Mater.*, 2019, **31**, 3957–3966.

205 Z. Li, X. Xu, W. Zhang, Z. Genene, W. Mammo, A. Yartsev, M. R. Andersson, R. A. J. Janssen and E. Wang, *J. Mater. Chem. A*, 2017, **5**, 11693–11700.
206 H.-J. Yun, J. Cho, D. S. Chung, Y.-H. Kim and S.-K. Kwon, *Macromolecules*, 2014, **47**, 7030–7035.
207 J. Lee, A.-R. Han, J. Kim, Y. Kim, J. H. Oh and C. Yang, *J. Am. Chem. Soc.*, 2012, **134**, 20713–20721.
208 S.-C. Chen, Q. Zheng, Q. Zhang, D. Cai, J. Wang, Z. Yin and C. Tang, *J. Polym. Sci., Part A: Polym. Chem.*, 2013, **51**, 1999–2005.
209 Z. Wang, Y. Shi, Y. Deng, Y. Han and Y. Geng, *Adv. Funct. Mater.*, 2021, **31**, 2104881.
210 D. Gao, Z. Chen, Z. Mao, J. Huang, W. Zhang, D. Li and G. Yu, *RSC Adv.*, 2016, **6**, 78008–78016.
211 X. Yan, M. Xiong, X.-Y. Deng, K.-K. Liu, J.-T. Li, X.-Q. Wang, S. Zhang, N. Prine, Z. Zhang, W. Huang, Y. Wang, J.-Y. Wang, X. Gu, S. K. So, J. Zhu and T. Lei, *Nat. Commun.*, 2021, **12**, 5723.
212 X. Yan, M. Xiong, J.-T. Li, S. Zhang, Z. Ahmad, Y. Lu, Z.-Y. Wang, Z.-F. Yao, J.-Y. Wang, X. Gu and T. Lei, *J. Am. Chem. Soc.*, 2019, **141**, 20215–20221.
213 X. Guo and M. D. Watson, *Org. Lett.*, 2008, **10**, 5333–5336.
214 Z. Chen, Y. Zheng, H. Yan and A. Facchetti, *J. Am. Chem. Soc.*, 2009, **131**, 8–9.
215 N. Zhou and A. Facchetti, *Mater. Today*, 2018, **21**, 377–390.
216 H. Yan, Z. Chen, Y. Zheng, C. Newman, J. R. Quinn, F. Dötz, M. Kastler and A. Facchetti, *Nature*, 2009, **457**, 679–686.
217 S. G. Bucella, A. Luzio, E. Gann, L. Thomsen, C. R. McNeill, G. Pace, A. Perinot, Z. Chen, A. Facchetti and M. Caironi, *Nat. Commun.*, 2015, **6**, 8394.
218 R. Matsidik, H. Komber, A. Luzio, M. Caironi and M. Sommer, *J. Am. Chem. Soc.*, 2015, **137**, 6705–6711.
219 R. Matsidik, H. Komber and M. Sommer, *ACS Macro Lett.*, 2015, **4**, 1346–1350.
220 J. W. Jung, J. W. Jo, C.-C. Chueh, F. Liu, W. H. Jo, T. P. Russell and A. K.-Y. Jen, *Adv. Mater.*, 2015, **27**, 3310–3317.
221 Z. Li, X. Xu, W. Zhang, X. Meng, W. Ma, A. Yartsev, O. Inganäs, M. R. Andersson, R. A. J. Janssen and E. Wang, *J. Am. Chem. Soc.*, 2016, **138**, 10935–10944.
222 Z. Li, X. Xu, W. Zhang, X. Meng, Z. Genene, W. Ma, W. Mammo, A. Yartsev, M. R. Andersson, R. A. J. Janssen and E. Wang, *Energy Environ. Sci.*, 2017, **10**, 2212–2221.
223 M. J. Sung, A. Luzio, W.-T. Park, R. Kim, E. Gann, F. Maddalena, G. Pace, Y. Xu, D. Natali, C. de Falco, L. Dang, C. R. McNeill, M. Caironi, Y.-Y. Noh and Y.-H. Kim, *Adv. Funct. Mater.*, 2016, **26**, 4984–4997.
224 K. Park, E.-Y. Shin, X. Jiao, C. R. McNeill, Y.-H. Kim, S.-K. Kwon and Y.-Y. Noh, *ACS Appl. Mater. Interfaces*, 2019, **11**, 35185–35192.
225 V. Senkovskyy, R. Tkachov, H. Komber, M. Sommer, M. Heuken, B. Voit, W. T. S. Huck, V. Kataev, A. Petr and A. Kiriy, *J. Am. Chem. Soc.*, 2011, **133**, 19966–19970.
226 R. Tkachov, Y. Karpov, V. Senkovskyy, I. Raguzin, J. Zessin, A. Lederer, M. Stamm, B. Voit, T. Beryozkina, V. Bakulev, W. Zhao, A. Facchetti and A. Kiriy, *Macromolecules*, 2014, **47**, 3845–3851.
227 M. Schubert, D. Dolfen, J. Frisch, S. Roland, R. Steyrleuthner, B. Stiller, Z. Chen, U. Scherf, N. Koch, A. Facchetti and D. Neher, *Adv. Energy Mater.*, 2012, **2**, 369–380.
228 L. Xue, Y. Yang, Z.-G. Zhang, X. Dong, L. Gao, H. Bin, J. Zhang, Y. Yang and Y. Li, *J. Mater. Chem. A*, 2016, **4**, 5810–5816.
229 S. Lee, C. Lee, H. Kim and Y. Kim, *J. Mater. Chem. C*, 2020, **8**, 15778–15787.
230 M.-K. Jeong, E. H. Suh, K. Lee, J. Jang and I. H. Jung, *Org. Electron.*, 2020, **86**, 105921.
231 F. Liu, H. Li, Y. Wu, C. Gu and H. Fu, *RSC Adv.*, 2015, **5**, 92151–92158.
232 K. Nakano, M. Nakano, B. Xiao, E. Zhou, K. Suzuki, I. Osaka, K. Takimiya and K. Tajima, *Macromolecules*, 2016, **49**, 1752–1760.
233 J. Yang, B. Xiao, K. Tajima, M. Nakano, K. Takimiya, A. Tang and E. Zhou, *Macromolecules*, 2017, **50**, 3179–3185.
234 Z. Zhao, F. Zhang, Y. Hu, Z. Wang, B. Leng, X. Gao, C. Di and D. Zhu, *ACS Macro Lett.*, 2014, **3**, 1174–1177.
235 Y. Fukutomi, M. Nakano, J.-Y. Hu, I. Osaka and K. Takimiya, *J. Am. Chem. Soc.*, 2013, **135**, 11445–11448.
236 H. A. M. van Mullekom, J. A. J. M. Venkemans and E. W. Meijer, *Chem. Commun.*, 1996, 2163–2164.
237 P. Cong, Z. Wang, Y. Geng, Y. Meng, C. Meng, L. Chen, A. Tang and E. Zhou, *Nano Energy*, 2023, **105**, 108017.
238 Y. Wang and T. Michinobu, *J. Mater. Chem. C*, 2016, **4**, 6200–6214.
239 P. Sonar, S. P. Singh, Y. Li, M. S. Soh and A. Dodabalapur, *Adv. Mater.*, 2010, **22**, 5409–5413.
240 J. Lee, M. Jang, S. M. Lee, D. Yoo, T. J. Shin, J. H. Oh and C. Yang, *ACS Appl. Mater. Interfaces*, 2014, **6**, 20390–20399.
241 J. Kim, A.-R. Han, J. Hong, G. Kim, J. Lee, T. J. Shin, J. H. Oh and C. Yang, *Chem. Mater.*, 2014, **26**, 4933–4942.
242 L. Ma, Z. Li, B. Chen, P. Xue, Z. Wang, Y. Wu, X. Zhan, Y. Liu and X. Chen, *Adv. Electron. Mater.*, 2022, **8**, 2101297.
243 K. Feng, Z. Wu, M. Su, S. Ma, Y. Shi, K. Yang, Y. Wang, Y. Zhang, W. Sun, X. Cheng, L. Huang, J. Min, H. Y. Woo and X. Guo, *Adv. Funct. Mater.*, 2021, **31**, 2008494.
244 D. Nodari, S. Sharma, W. Jia, A. V. Marsh, Y.-H. Lin, Y. Fu, X. Lu, A. Russkikh, G. T. Harrison, S. Fatayer, N. Gasparini, M. Heeney and J. Panidi, *Adv. Mater.*, 2024, 2402568.
245 C. N. Scott, M. D. Bisen, D. M. Stemer, S. McKinnon and C. K. Luscombe, *Macromolecules*, 2017, **50**, 4623–4628.
246 J. D. Yuen, J. Fan, J. Seifter, B. Lim, R. Hufschmid, A. J. Heeger and F. Wudl, *J. Am. Chem. Soc.*, 2011, **133**, 20799–20807.
247 Y. Wang, M. Nakano, T. Michinobu, Y. Kiyota, T. Mori and K. Takimiya, *Macromolecules*, 2017, **50**, 857–864.
248 C. Zhang, J. Zhang, W. Zeng, N. Zheng, W. Li, W. Gao, G. Yu and C. Yang, *Polym. Chem.*, 2016, **7**, 2808–2814.
249 H. Chen, G. Cai, A. Guo, Z. Zhao, J. Kuang, L. Zheng, L. Zhao, J. Chen, Y. Guo and Y. Liu, *Macromolecules*, 2019, **52**, 6149–6159.

250 C. An, S. R. Puniredd, X. Guo, T. Stelzig, Y. Zhao, W. Pisula and M. Baumgarten, *Macromolecules*, 2014, **47**, 979–986.
251 Y. Dong, W. Cai, X. Hu, C. Zhong, F. Huang and Y. Cao, *Polymer*, 2012, **53**, 1465–1472.
252 X. Hu, Y. Dong, F. Huang, X. Gong and Y. Cao, *J. Phys. Chem. C*, 2013, **117**, 6537–6543.
253 S. Cho, J. Lee, M. Tong, J. H. Seo and C. Yang, *Adv. Funct. Mater.*, 2011, **21**, 1910–1916.
254 J. Park, C. Lee, T. Kim, H. Kim and Y. Kim, *Adv. Electron. Mater.*, 2021, **7**, 2000932.
255 Q. Li, Y. Ran, W. Shi, M. Qin, Y. Sun, J. Kuang, H. Wang, H. Chen, Y. Guo and Y. Liu, *Appl. Mater. Today*, 2021, **22**, 100899.
256 X. Liu, M. Sha, H. Yin and X. Hao, *APL Energy*, 2023, **1**, 031501.
257 Y. Zhang, Y. Ji, Y. Zhang, W. Zhang, H. Bai, M. Du, H. Wu, Q. Guo and E. Zhou, *Adv. Funct. Mater.*, 2022, **32**, 2205115.
258 P. Xue, P. Cheng, R. P. S. Han and X. Zhan, *Mater. Horiz.*, 2021, **9**, 194–219.
259 F. Zhao, H. Zhang, R. Zhang, J. Yuan, D. He, Y. Zou and F. Gao, *Adv. Energy Mater.*, 2020, **10**, 2002746.
260 D. Li, X. Zhang, D. Liu and T. Wang, *J. Mater. Chem. A*, 2020, **8**, 15607–15619.
261 Y. Meng, J. Wu, X. Guo, W. Su, L. Zhu, J. Fang, Z.-G. Zhang, F. Liu, M. Zhang, T. P. Russell and Y. Li, *Sci. China Chem.*, 2019, **62**, 845–850.
262 T. Jia, J. Zhang, W. Zhong, Y. Liang, K. Zhang, S. Dong, L. Ying, F. Liu, X. Wang, F. Huang and Y. Cao, *Nano Energy*, 2020, **72**, 104718.
263 Q. Fan, H. Fu, M. Liu, J. Oh, X. Ma, F. R. Lin, C. Yang, F. Zhang and A. K.-Y. Jen, *ACS Appl. Mater. Interfaces*, 2022, **14**, 26970–26977.
264 H. Lai, H. Chen, Y. Zhu, H. Wang, Y. Li and F. He, *Macromolecules*, 2022, **55**, 3353–3360.
265 Z. Luo, T. Liu, R. Ma, Y. Xiao, L. Zhan, G. Zhang, H. Sun, F. Ni, G. Chai, J. Wang, C. Zhong, Y. Zou, X. Guo, X. Lu, H. Chen, H. Yan and C. Yang, *Adv. Mater.*, 2020, **32**, 2005942.
266 H. Yu, M. Pan, R. Sun, I. Agunawela, J. Zhang, Y. Li, Z. Qi, H. Han, X. Zou, W. Zhou, S. Chen, J. Y. L. Lai, S. Luo, Z. Luo, D. Zhao, X. Lu, H. Ade, F. Huang, J. Min and H. Yan, *Angew. Chem., Int. Ed.*, 2021, **60**, 10137–10146.
267 T. Wang, R. Sun, W. Wang, H. Li, Y. Wu and J. Min, *Chem. Mater.*, 2021, **33**, 761–773.
268 X. Yang, R. Sun, Y. Wang, M. Chen, X. Xia, X. Lu, G. Lu and J. Min, *Adv. Mater.*, 2023, **35**, 2209350.
269 Q. Fan, H. Fu, Q. Wu, Z. Wu, F. Lin, Z. Zhu, J. Min, H. Y. Woo and A. K.-Y. Jen, *Angew. Chem., Int. Ed.*, 2021, **60**, 15935–15943.
270 H. Fu, Y. Li, J. Yu, Z. Wu, Q. Fan, F. Lin, H. Y. Woo, F. Gao, Z. Zhu and A. K.-Y. Jen, *J. Am. Chem. Soc.*, 2021, **143**, 2665–2670.
271 F. Qin, G. Li, Y. Liu, Y. Cho, R. M. Pankow, D. Zhang, L. Feng, Y. Wang, S. Jeong, G. Forti, D. Zheng, C. Yang, Y. Zhou, T. J. Marks and A. Facchetti, *ACS Energy Lett.*, 2023, **8**, 4733–4745.
272 Q. Fan, R. Ma, T. Liu, J. Yu, Y. Xiao, W. Su, G. Cai, Y. Li, W. Peng, T. Guo, Z. Luo, H. Sun, L. Hou, W. Zhu, X. Lu, F. Gao, E. Moons, D. Yu, H. Yan and E. Wang, *Sci. China Chem.*, 2021, **64**, 1380–1388.
273 S. Ma, B. Li, S. Gong, J. Wang, B. Liu, S. Young Jeong, X. Chen, H. Young Woo, K. Feng and X. Guo, *Angew. Chem., Int. Ed.*, 2023, **62**, e202308306.
274 W. Feng, T. Chen, Y. Li, T. Duan, X. Jiang, C. Zhong, Y. Zhang, J. Yu, G. Lu, X. Wan, B. Kan and Y. Chen, *Angew. Chem., Int. Ed.*, 2024, **63**, e202316698.
275 G. Forti, R. M. Pankow, F. Qin, Y. Cho, B. Kerwin, I. Duplessis, A. Nitti, S. Jeong, C. Yang, A. Facchetti, D. Pasini and T. J. Marks, *Chem. – Eur. J.*, 2023, **29**, e202300653.
276 J. Zhang, C.-H. Tan, K. Zhang, T. Jia, Y. Cui, W. Deng, X. Liao, H. Wu, Q. Xu, F. Huang and Y. Cao, *Adv. Energy Mater.*, 2021, **11**, 2102559.
277 Y. Zhao, X. Zhao, Y. Zang, C. Di, Y. Diao and J. Mei, *Macromolecules*, 2015, **48**, 2048–2053.
278 E. L. Melenbrink, K. M. Hilby, M. A. Alkhadra, S. Samal, D. J. Lipomi and B. C. Thompson, *ACS Appl. Mater. Interfaces*, 2018, **10**, 32426–32434.
279 R. Po, G. Bianchi, C. Carbonera and A. Pellegrino, *Macromolecules*, 2015, **48**, 453–461.
280 S. Park, Y. Kim, C. Choi, H. Ahn, T. Park, S. H. Lee, Y. H. Jang and B. H. Lee, *Macromol. Rapid Commun.*, 2022, **43**, 2100709.
281 S. Heo, J. Kwon, M. Sung, S. Lee, Y. Cho, H. Jung, I. You, C. Yang, J. Lee and Y.-Y. Noh, *ACS Appl. Mater. Interfaces*, 2023, **15**, 1629–1638.
282 L. Ying, B. B. Y. Hsu, H. Zhan, G. C. Welch, P. Zalar, L. A. Perez, E. J. Kramer, T.-Q. Nguyen, A. J. Heeger, W.-Y. Wong and G. C. Bazan, *J. Am. Chem. Soc.*, 2011, **133**, 18538–18541.
283 H. Yoo, M. Sung, H. Ahn, D. Yang, J. S. Yoo, J. Lee and B. H. Lee, *Chem. Mater.*, 2023, **35**, 9562–9571.
284 M. E. Foster, B. A. Zhang, D. Murtagh, Y. Liu, M. Y. Sfeir, B. M. Wong and J. D. Azoulay, *Macromol. Rapid Commun.*, 2014, **35**, 1516–1521.
285 A. E. London, L. Huang, B. A. Zhang, M. B. Oviedo, J. Tropp, W. Yao, Z. Wu, B. M. Wong, T. N. Ng and J. D. Azoulay, *Polym. Chem.*, 2017, **8**, 2922–2930.
286 W. Li, K. H. Hendriks, A. Furlan, M. M. Wienk and R. A. J. Janssen, *J. Am. Chem. Soc.*, 2015, **137**, 2231–2234.
287 J. Hou, H.-Y. Chen, S. Zhang, G. Li and Y. Yang, *J. Am. Chem. Soc.*, 2008, **130**, 16144–16145.
288 Z. Yang, Z. Liu and L. Chen, *ACS Appl. Polym. Mater.*, 2023, **5**, 7658–7665.
289 W. Yao, Z. Wu, E. Huang, L. Huang, A. E. London, Z. Liu, J. D. Azoulay and T. N. Ng, *ACS Appl. Electron. Mater.*, 2019, **1**, 660–666.
290 Z. Wu, W. Yao, A. E. London, J. D. Azoulay and T. N. Ng, *Adv. Funct. Mater.*, 2018, **28**, 1800391.
291 J. D. Azoulay, Z. A. Koretz, B. M. Wong and G. C. Bazan, *Macromolecules*, 2013, **46**, 1337–1342.
292 C. Park, J. M. Kim, Y. Kim, S. Bae, M. Do, S. Im, S. Yoo and J. H. Kim, *ACS Appl. Electron. Mater.*, 2021, **3**, 4781–4792.

293 K. Fukuda, K. Yu and T. Someya, *Adv. Energy Mater.*, 2020, **10**, 2000765.
294 S. Chang, J. H. Koo, J. Yoo, M. S. Kim, M. K. Choi, D.-H. Kim and Y. M. Song, *Chem. Rev.*, 2024, **124**, 768–859.
295 J. Fu, Q. Yang, P. Huang, S. Chung, K. Cho, Z. Kan, H. Liu, X. Lu, Y. Lang, H. Lai, F. He, P. W. K. Fong, S. Lu, Y. Yang, Z. Xiao and G. Li, *Nat. Commun.*, 2024, **15**, 1830.
296 Q. Wan, S. Seo, S.-W. Lee, J. Lee, H. Jeon, T.-S. Kim, B. J. Kim and B. C. Thompson, *J. Am. Chem. Soc.*, 2023, **145**, 11914–11920.
297 M. Y. Lee, S. Dharmapurikar, S. J. Lee, Y. Cho, C. Yang and J. H. Oh, *Chem. Mater.*, 2020, **32**, 1914–1924.
298 A. Nyayachavadi, A. K. Sur, P. Kulatunga, Y. Wang, T. C. Gomes, M. Mooney, G. T. Mason, A. Hu, X. Gu and S. Rondeau-Gagné, *Chem. Mater.*, 2023, **35**, 9682–9691.
299 G. G. Yang, D.-H. Kim, S. Samal, J. Choi, H. Roh, C. E. Cunin, H. M. Lee, S. O. Kim, M. Dincă and A. Gumyusenge, *ACS Sens.*, 2023, **8**, 3687–3692.
300 A. Gumyusenge, D. T. Tran, X. Luo, G. M. Pitch, Y. Zhao, K. A. Jenkins, T. J. Dunn, A. L. Ayzner, B. M. Savoie and J. Mei, *Science*, 2018, **362**, 1131–1134.
301 R. Ji, Y.-Q.-Q. Yi, X. Wang, X. Wu, C. Huang, W. Su and Z. Cui, *Thin Solid Films*, 2024, **790**, 140219.